Chapter 4. Stereochemistry and Electrochemical Property of S-Bridged Polynuclear Molybdenum Complexes

4-1. Introduction

It has been highly interested molybdenum polynuclear system, which contains sulfur coordination.[1-8] For example, large number of polynuclear structures involving the incomplete cuboidal molybdenum trinuclear clusters, $[Mo_3(\mu_3\text{-}S)\ (\mu\text{-}O)_{3-n}(\mu\text{-}S)_n]^{4+}$ (n = 0 - 3),[1,2] or the oxomolybdenum dinuclear units, $[Mo_2O_{2-m}S_m(\mu\text{-}O)_{2-n}(\mu\text{-}S)_n]^{2+}$ (m = 0 - 2, n = 0 - 2),[1,3] were extensively investigated. Especially, heteropolynuclear structures are also important biologically.[4] On the other hand, it has been known that molybdenum ion can take various valences and structures.[5] The complexes involving 0 to + 6 valent and 4 to 8 coordinated molybdenum ions are commonly known. Thus, polynuclear complexes containing molybdenum-sulfur bonds are interested in their stereochemistry and reactivity. However, the study of stereochemistry and reactivity around molybdenum ion has been little, due to stability or polymerization ability of the cluster moieties.[1,9]

It is worth to attempt the incorporation of molybdenum ion to S-bridged polynuclear structure, in order to explore stereochemistry and reactivity. In chapter 2, the S-bridged trinuclear complexes involving chromium(III) ion, which is early transition metal ion, were prepared.[10] These polynuclear chromium(III) complexes have indicated different reactivity and electrochemical property from the previously reported S-bridged polynuclear complexes, which consist of late transition metal ions. It has been known that molybdenum ion takes various valences and structures, and molybdenum ion has its highly different redox and stereochemical properties from chromium ion in spite of congeners. Thus, appearance of various interesting properties will be expected in S-bridged polynuclear molybdenum complexes.

In this chapter, I have paid attentions to molybdenum(III) complexes which are very rare because of its instability toward oxygen and attempted the reactions of *fac(S)*-$[M(aet)_3]$ (M = Ir^{III} and Rh^{III}) with $(NH_4)_2[Mo^{III}Cl_5(H_2O)]$.

Since molybdenum ion has been generally stabilized as high oxidation state, it is interesting whether molybdenum ion, which is incorporated into S-bridged polynuclear structure, retains starting trivalent state. On the other hand, molybdenum(IV) or molybdenum(V) complexes usually exist as molybdenum polynuclear unit and it is also intriguing whether such polynuclear unit is incorporated into S-bridged polynuclear structure by building blocks. I found plural S-bridged polynuclear complexes, whose valence and structure are different from others depending upon building blocks. Namely, linear-type S-bridged trinuclear complexes, $[Mo^{IV}\{Ir(aet)_3\}_2]^{4+}$ (5) and $[Mo^{III}\{Rh(aet)_3\}_2]^{3+}$ (6), and unprecedented S-bridged pentanuclear complex, $[Mo^{V}_2O_3\{Rh(aet)_3\}_3]^{4+}$ (7), were prepared by the reactions of the molybdenum(III) ion with *fac(S)*-$[M(aet)_3]$ ($M = Ir^{III}$ and Rh^{III}). A reaction of *fac(S)*-$[Co(aet)_3]$ with molybdenum(V) ion was also attempted, and S-bridged tetranuclear complex, $[Mo^{V}_2O_4\{Co(aet)_3\}_2]^{2+}$ (8) was obtained. The crystal structures of the obtained complexes **5** - **7** and *ΔΛ*-$[M'\{Rh(aet)_3\}_2]^{3+}$ ($M' = Fe^{III}$ (9), Co^{III} (10)),[11,12] which are for the purpose of comparison, were determined by an X-ray diffraction study. The stereochemistry and spectrochemical behavior of these complexes are investigated. The electrochemical property and structural change for the present complexes are also discussed. Finally, the relationship between the structure and the spectroscopy for the linear-type trinuclear complexes is described.

4-2. Experimental

4-2-1. Materials

All chemicals were purchased from the companies as described in chapter 2. They were of reagent grade, and were used without further purification.

4-2-2. Preparation of Complexes

$(NH_4)_2[Mo^{III}Cl_5(H_2O)]$ This complex was prepared by a modified

method of Shibahara et al.[13] In this literature, the preparation method of $(NH_4)_3[Mo^{III}Cl_6]$ was described. $(NH_4)_2[Mo^{III}Cl_5(H_2O)]$ was produced instead of $(NH_4)_3[Mo^{III}Cl_6]$ without HCl gas.

$Cs_2[Mo^{V}OCl_5]$ This complex was prepared by the general procedure. $MoCl_5$ (3.00 g, 10.98 mmol) was dissolved slowly in 5 cm^3 of 4 mol dm^{-3} HCl under nitrogen atmosphere. After the brown mixture was cooled to room temperature, added CsCl (3.70 g, 21.98 mmol) in 2 cm^3 of water, and stood in a refrigerator for 15 min. The resulting green powder was collected by filtration. Yield: 5.14 g (84 %).

***fac(S)*-[Ir(aet)$_3$], *fac(S)*-[Rh(aet)$_3$], *fac(S)*-[Co(aet)$_3$], and *fac(S)*-[Cr(aet)$_3$]** These complexes were prepared by the methods described in chapter 2.

$[Mo^{IV}\{Ir(aet)_3\}_2]^{4+}$ (5) $(NH_4)_2[Mo^{III}Cl_5(H_2O)]$ (0.118 g, 0.361 mmol) was dissolved in 3 cm^3 of 1 mol dm^{-3} HBr and added 1 cm^3 of a saturated NaBr aqueous solution. To the red solution was added *fac(S)*-$[Ir(aet)_3]$ (0.300 g, 0.713 mmol) slowly with stirring. The orange mixture was stirred under nitrogen atmosphere at room temperature for 15 min, whereupon it became a dark brown suspension. The resulting dark brown crystalline powder ($5Br_4 \cdot 4H_2O$) were collected by filtration. Yield: 0.411 g (87 %). Similar crystalline powder was also obtained by a reaction under air atmosphere. Single crystals suitable for X-ray analysis were obtained by recrystallization from water by adding a few drops of a saturated NaBr aqueous solution. Found: C, 10.92; H, 3.40; N, 6.21; Mo, 6.86; Ir, 28.58 %. Calcd for $[Mo\{Ir(aet)_3\}_2]Br_4 \cdot 4H_2O = C_{12}H_{36}N_6S_6Br_4MoIr_2 \cdot 4H_2O$: C, 10.85; H, 3.34; N, 6.32; Mo, 7.22; Ir, 28.93 %.

$[Mo^{III}\{Rh(aet)_3\}_2]^{3+}$ (6) *fac(S)*-$[Rh(aet)_3]$ (0.300 g, 0.905 mmol) was dissolved in 5 cm^3 of 1 mol dm^{-3} HBr. To the yellow solution was added $(NH_4)_2[Mo^{III}Cl_5(H_2O)]$ (0.150 g, 0.458 mmol) in 2 cm^3 of 1 mol dm^{-3} HBr. The orange mixture was stirred under nitrogen atmosphere at room temperature for 15 min, whereupon it became a green-brown suspension. To this suspension was added 1 cm^3 of a saturated NaBr aqueous solution, followed by stirring for 15 min. After standing in a refrigerator for 3 h, the

resulting black micro crystals ($6Br_3 \cdot H_2O$) were collected by filtration. Yield: 0.422 g (92 %). Similar micro crystals were also obtained by a reaction under air atmosphere. Single crystals suitable for X-ray analysis were obtained by recrystallization from water by adding a few drops of a saturated NaBr aqueous solution. Found: C, 14.05; H, 3.72; N, 8.22; Mo, 9.05; Rh, 19.92 %. Calcd for $[Mo\{Rh(aet)_3\}_2]Br_3 \cdot H_2O = C_{12}H_{36}N_6S_6Br_3MoRh_2 \cdot H_2O$: C, 14.18; H, 3.77; N, 8.27; Mo, 9.44; Rh, 20.25 %.

$[Mo^{V}_2O_3\{Rh(aet)_3\}_3]^{4+}$ (7) *Method A:* $6Br_3 \cdot H_2O$ (0.420 g, 0.413 mmol) was dissolved in 30 cm^3 of water, and added a few drops of a saturated NaBr aqueous solution. After standing in a refrigerator for 3 d, unsolved precipitate was removed by filtration. To the resulting wine-red filtrate was added 1 cm^3 of a saturated NaBr aqueous solution. Black crystals ($7Br_4 \cdot 6H_2O$) were appeared by standing in a refrigerator for further 3 d. Yield: 0.247 g (72 %).

Method B: *fac(S)*-$[Rh(aet)_3]$ (0.300 g, 0.905 mmol) was dissolved in 5 cm^3 of 1 mol dm^{-3} HBr. To the yellow solution was added $(NH_4)_2[Mo^{III}Cl_5(H_2O)]$ (0.300 g, 0.917 mmol) in 5 cm^3 of 1 mol dm^{-3} HBr. The orange mixture was stirred under air atmosphere at room temperature for 1 d, whereupon it became a wine-red suspension. After added 1 cm^3 of a saturated NaBr aqueous solution and stirred for 1 d, the resulting wine-red powder (0.503 g) was collected by filtration. To the rough powder was added 50 cm^3 of water and insoluble materials were removed by filtration. To the wine-red filtrate added 3 cm^3 of a saturated NaBr aqueous solution. The resulting black micro crystals ($7Br_4 \cdot 6H_2O$) were collected by filtration. Yield: 0.133 g (27 %).

Single crystals suitable for X-ray analysis were obtained by recrystallization from water by adding a few drops of a saturated NaBr aqueous solution. Found: C, 12.87; H, 4.04; N, 7.47; Mo, 10.39; Rh, 18.25 %. Calcd for $[Mo_2O_3\{Rh(aet)_3\}_3]Br_4 \cdot 6H_2O = C_{18}H_{54}N_9O_3S_9Br_4Mo_2Rh_3 \cdot 6H_2O$: C, 13.01; H, 4.00; N, 7.59; Mo, 11.55; Rh, 18.58 %.

$[Mo^{V}_2O_4\{Co(aet)_3\}_3]^{2+}$ (8) To a suspension containing 1.00 g (3.48

mmol) of *fac(S)*-[Co(aet)$_3$] in 20 cm^3 of water was added 1.00 g (3.66 mmol) of $MoCl_5$ in 20 cm^3 of water. The dark brown mixture was stirred at room temperature for 15 min, whereupon it formed a brown precipitate. The resulting brown powder (1.33 g) was collected by filtration and washed with acetone. Similar brown powder was obtained by using $Cs_2[Mo^VOCl_5]$ instead of $MoCl_5$. 0.50 g of rough powder was dissolved in 100 cm^3 of water and insoluble materials were removed by filtration. The resulting brown micro crystals ($8(NO_3)_2 \cdot 3H_2O$) were appeared by adding 5 cm^3 of a saturated $NaNO_3$ aqueous solution. Yield: 0.23 g (35 %). Found: C, 14.32; H, 4.18; N, 11.13; Mo, 18.18; Co, 11.04 %. Calcd for $[Mo_2O_4\{Co(aet)_3\}_2](NO_3)_2 \cdot 4H_2O = C_{12}H_{36}N_8O_{10}S_6Co_2Mo_2 \cdot 3H_2O$: C, 14.29; H, 4.20; N, 11.11; Mo, 19.02; Co, 11.69 %.

***ΔΛ*-[Fe{Rh(aet)$_3$}$_2$]$^{3+}$ (9) and *ΔΛ*-[Co{Rh(aet)$_3$}$_2$]$^{3+}$ (10)** These complexes were prepared by the methods described in the literatures,[11,12] and recrystallized from water by adding a few drops of a saturated $NaNO_3$ aqueous solution. One of the crystals was used for X-ray structural analysis.

4-2-3. Measurements

The electronic absorption spectra were recorded with a JASCO V-560 spectrophotometer. All the measurements were carried out in aqueous solution at room temperature. The elemental analyses (C, H, N) were performed by the Analysis Center of the University of Tsukuba. The concentrations of Mo, Ir, Rh, and Co in their complexes were determined with a NIPPON Jarrell-Ash ICPA-575 ICP spectrophotometer. The diffuse reflectance spectra were recorded with a JASCO V-570 spectrophotometer. The infrared spectra were recorded as a KBr disk with a JASCO FT/IR-550 spectrometer. The Raman spectra were recorded on a JASCO R-800 laser Raman spectrophotometer with an excitation by Ar^+ ion laser line, 514.5 nm, and the samples were in the form of a KBr disk. The ^{13}C NMR spectra (125.759 MHz) were recorded with a BRUKER AM-500 NMR spectrometer in D_2O. The sodium 4,4-dimethyl-4-silapentane-1-sulfonate (DSS) was used as an internal reference. The molar conductances of the complexes were

measured with a HORIBA conductivity.meter DS-14 in aqueous solution at room temperature. The magnetic measurements were performed by using a Sherwood Scientific apparatus at 23 °C. Diamagnetic corrections were obtained employing tabulated constants.[14] Electrochemical measurements were made by CV-1B apparatus (Biochemical Systems, Inc.) using a grassy-carbon working electrode (Biochemical Systems, Inc., GCE). An aqueous Ag/AgCl/NaCl (3 mol dm^{-3}) electrode (Biochemical Systems, Inc., RE-1) and platinum wire were used as reference and auxiliary electrode, respectively. Electrochemical experiments were conducted in a 0.1 mol dm^{-3} aqueous solution of Na_2SO_4 as a supporting electrolyte and complex concentrations of 1.0 mmol dm^{-3}. Molecular Mechanics calculations (MM2 program) were performed on a Power Macintosh computer with CAChe program.[15]

The structural change for the complex with times was carried out by the absorption spectral measurements. A solution containing 0.0075 g of $[Mo^{III}\{Rh(aet)_3\}_2]^{3+}$ (6) in 0.5 cm^3 of water was exposed to air with stirring at room temperature for the definite time. These solution were filtered and the filtrate were diluted to 25 cm^3 by of 1 mol dm^{-3} HCl solution, the absorption spectra were measured on a JASCO V-560 spectrophotometer.

4-2-4. Crystallography

Single crystals of $5Br_4 \cdot 4H_2O$, $6Br_3 \cdot H_2O$, $7Br_4 \cdot 6H_2O$, $9(NO_3)_3 \cdot 4H_2O$, and $10(NO_3)_3 \cdot 3H_2O$ were used for data collection on Rigaku AFC-7S four-circle diffractometer with graphite-monochromatized Mo $K\alpha$ (0.71069 Å) radiation. Unit cell parameters were determined by least-squares refinements of 25 reflections. Crystallographic data and experimental parameters are summarized in Tables 4-1, 4-2 and 4-3. The intensity data were collected by the ω - 2θ scan technique, and the scan rate varied from 1 to 5 ° min^{-1} (on ω). The intensities were corrected for Lorentz and polarization. An empirical absorption correction based on a series of ψ scans was applied. The independent reflections ($I_0 > 5.0\sigma(I_0)$ for 6; $I_0 > 3.0\sigma(I_0)$ for the others) were used for the structure determinations. The positions of the Ir, Rh, and some other atoms were determined by the direct method (SAPI91[16] for 5 and 6;

SIR92[17] for the others). The difference Fourier maps based on these atomic positions revealed the other non-hydrogen atoms. The structures were refined by full-matrix least-squares refinements on F of the positional parameters and the anisotropic thermal parameters of the non-hydrogen atoms in $\mathbf{5}Br_4 \cdot 4H_2O$, $\mathbf{6}Br_3 \cdot H_2O$, $\mathbf{7}Br_4 \cdot 6H_2O$, $\mathbf{9}(NO_3)_3 \cdot 4H_2O$, or $\mathbf{10}(NO_3)_3 \cdot 3H_2O$. The hydrogen atoms on the aet ligands were fixed by the geometrical and thermal constrains (C-H = N-H = 0.95 Å and $U = 1.3U(C,N)$). The occupancy factors (Occ) for some atoms are listed in Tables 4-4, 4-5, 4-6, 4-7, and 4-8. In $\mathbf{6}Br_3 \cdot H_2O$, two sets of atom peaks corresponding to a pair of enantiomers co-exist in unit cell, and refined using isotropic thermal parameters for some non-hydrogen atoms (Table 4-5). All the calculations were performed on an

Table 4-1. Crystallographic Data for $[Mo\{Ir(aet)_3\}_2]Br_4 \cdot 4H_2O$ ($\mathbf{5}Br_4 \cdot 4H_2O$) and $[Mo\{Rh(aet)_3\}_2]Br_3 \cdot H_2O$ ($\mathbf{6}Br_3 \cdot H_2O$)

	5	**6**
Formula	$C_{12}H_{44}Br_4N_6O_4S_6Ir_2Mo$	$C_{12}H_{38}Br_3N_6OS_6MoRh_2$
Formula weight	1328.87	1016.29
Cryst. dimens / mm	0.43 x 0.13 x 0.13	0.20 x 0.20 x 0.20
Cryst. system	Monoclinic	Orthorhombic
Space group	$P2_1/n$ (No. 14)	*P*nma (No. 62)
a / Å	11.530(3)	17.125(7)
b / Å	12.026(2)	12.450(5)
c / Å	12.577(2)	14.184(4)
β / °	90.45(2)	
V / Å^3	1743.9(6)	3024(1)
Z	2	4
D_{calcd} / g cm^{-3}	2.530	2.232
μ(Mo $K\alpha$) / cm^{-1}	129.71	58.92
Transm. coeff.	0.7034 - 1.0000	0.5826 - 0.9690
Temp. / K	296	296
No. of measd reflcns	4204	3899
No. of reflcns for used	2597 ($I_0 > 3.0\sigma(I_0)$)	1031 ($I_0 > 5.0\sigma(I_0)$)
No. of parameters	160	197
Final R	0.072	0.049
Final R_w	0.095	0.064
GOF	2.29	1.37

Table 4-2. Crystallographic Data for $[Mo_2O_3\{Rh(aet)_3\}_3]Br_4 \cdot 6H_2O$ ($7Br_4 \cdot 6H_2O$)

	7
Formula	$C_{18}H_{66}Br_4N_9O_9S_9Mo_2Rh_3$
Formula weight	1661.53
Cryst. dimens / mm	0.35 x 0.10 x 0.04
Cryst. system	Triclinic
Space group	$P\bar{1}$ (No. 2)
a / Å	14.236(5)
b / Å	14.917(3)
c / Å	13.622(2)
α / °	114.81(1)
β / °	95.57(2)
γ / °	82.46(3)
V / Å^3	2600(1)
Z	2
D_{calcd} / g cm^{-3}	2.122
μ(Mo $K\alpha$) / cm^{-1}	48.89
Transm. coeff.	0.7947 - 0.9972
Temp. / K	296
No. of measd reflcns	11954
No. of reflcns for used	5987 ($I_0 > 3.0\sigma(I_0)$)
No. of parameters	466
Final R	0.043
Final R_w	0.055
GOF	1.34

Table 4-3. Crystallographic Data for $[Fe\{Rh(aet)_3\}_2](NO_3)_3 \cdot 4H_2O$ ($9(NO_3)_3 \cdot 4H_2O$) and $[Co\{Rh(aet)_3\}_2](NO_3)_3 \cdot 3H_2O$ ($10(NO_3)_3 \cdot 3H_2O$)

	9	10
Formula	$C_{12}H_{44}N_9O_{13}S_6FeRh_2$	$C_{12}H_{42}N_9O_{12}S_6CoRh_2$
Formula weight	976.55	961.62
Cryst. dimens / mm	0.10 x 0.13 x 0.25	0.13 x 0.23 x 0.43
Cryst. system	Triclinic	Triclinic
Space group	$P\bar{1}$ (No. 2)	$P\bar{1}$ (No. 2)
a / Å	8.975(1)	8.974(3)
b / Å	12.031(2)	12.043(4)
c / Å	8.866(1)	8.849(3)

Table 4-3. Continued.

	9	10
α / °	110.53(1)	110.17(2)
β / °	102.66(1)	102.95(2)
γ / °	70.592(10)	70.80(3)
V / Å^3	839.9(2)	841.2(5)
Z	1	1
D_{calcd} / g cm^{-3}	1.930	1.898
μ(Mo $K\alpha$) / cm^{-1}	18.34	18.90
Transm. coeff.	0.8902 - 0.9998	0.9220 - 0.9982
Temp. / K	296	296
No. of measd reflcns	3859	1986
No. of reflcns for used	3107 ($I_0 > 3.0\sigma(I_0)$)	1715 ($I_0 > 3.0\sigma(I_0)$)
No. of parameters	205	207
Final R	0.048	0.043
Final R_w	0.082	0.076
GOF	1.62	0.76

Indigo II computer using the teXsan crystallographic software package.[18] The final atomic coordinates for non-hydrogen atoms are also given in Tables 4-4, 4-5, 4-6, 4-7, and 4-8.

Table 4-4. Final Atomic Coordinates, Equivalent Isotropic Thermal Parameters (B_{eq} / Å),[a] and Occupancy Factors (Occ) for Non-Hydrogen Atoms of $[Mo\{Ir(aet)_3\}_2]Br_4 \cdot 4H_2O$ ($5Br_4 \cdot 4H_2O$)

Atom	x	y	z	B_{eq}	Occ
Ir(1)	0.46744(7)	0.62447(6)	0.68169(6)	2.43(2)	
Mo(1)	0.5000	0.5000	0.5000	2.63(5)	0.5
S(1)	0.6418(6)	0.6224(6)	0.5877(5)	4.4(1)	
S(2)	0.4454(6)	0.4298(5)	0.6760(5)	4.3(1)	
S(3)	0.3548(6)	0.6493(5)	0.5259(5)	4.4(1)	
N(1)	0.488(2)	0.797(2)	0.688(2)	4.5(5)	
N(2)	0.558(2)	0.595(2)	0.824(2)	4.3(5)	
N(3)	0.307(2)	0.637(2)	0.760(2)	4.9(5)	

Table 4-4. Continued.

Atom	x	y	z	B_{eq}	Occ
C(1)	0.630(2)	0.766(2)	0.544(2)	3.9(5)	
C(2)	0.606(2)	0.834(2)	0.645(2)	4.4(6)	
C(3)	0.566(2)	0.400(2)	0.762(2)	3.7(5)	
C(4)	0.553(2)	0.471(2)	0.859(2)	4.4(6)	
C(5)	0.219(2)	0.601(2)	0.588(2)	3.5(5)	
C(6)	0.209(2)	0.667(2)	0.685(2)	3.8(5)	
Br(1)	0.4299(2)	0.8054(2)	0.9554(2)	4.39(6)	
Br(2)	0.2916(3)	0.9544(2)	0.5690(2)	4.96(6)	
O(1w)	0.310(2)	0.851(2)	0.319(1)	5.6(5)	
O(2w)	0.573(2)	1.023(2)	0.835(2)	7.9(7)	

a) B_{eq} denotes the equivalent isotropic temperature factors, $B_{eq} = (8\pi^2/3)\Sigma\Sigma U_{ij}a^*_i a^*_j \boldsymbol{a}_i \cdot \boldsymbol{a}_j$

Table 4-5. Final Atomic Coordinates, Equivalent Isotropic Thermal Parameters (B_{eq} / Å),[a] and Occupancy Factors (Occ) for Non-Hydrogen Atoms of $[Mo\{Rh(aet)_3\}_2]Br_3 \cdot H_2O$ ($6Br_3 \cdot H_2O$)

Atom	x	y	z	B_{eq}	Occ
Rh(1)	0.5063(1)	0.7500	0.8016(1)	3.24(5)	0.5
Rh(2)	0.3865(1)	0.7500	0.4252(1)	4.27(6)	0.5
Mo(1)	0.4455(2)	0.7500	0.6144(2)	3.46(6)	0.5
S(1)	0.3866(6)	0.6714(8)	0.7549(6)	3.9(2)	0.5
S(2)	0.4795(6)	0.9007(7)	0.7158(6)	3.2(2)	0.5
S(3)	0.5649(5)	0.6665(8)	0.6712(6)	3.5(2)	0.5
S(4)	0.5021(7)	0.8410(8)	0.4791(7)	4.3(3)	0.5
S(5)	0.4239(7)	0.6022(8)	0.5008(7)	4.3(3)	0.5
S(6)	0.3190(6)	0.8123(8)	0.5595(6)	4.0(2)	0.5
N(1)	0.523(2)	0.602(2)	0.880(2)	3.1(6)[b]	0.5
N(2)	0.453(2)	0.825(3)	0.913(2)	4.0(8)	0.5
N(3)	0.613(2)	0.805(2)	0.838(2)	3.8(7)	0.5
N(4)	0.455(2)	0.7500	0.307(2)	11(1)	0.5
N(5)	0.288(2)	0.671(4)	0.383(3)	7(1)	0.5
N(6)	0.351(2)	0.906(4)	0.368(2)	7(1)	0.5
C(1)	0.419(2)	0.531(3)	0.782(3)	3.3(9)[b]	0.5
C(2)	0.455(3)	0.538(4)	0.881(3)	3.9(9)[b]	0.5
C(3)	0.399(2)	0.939(3)	0.798(3)	2.7(8)[b]	0.5
C(4)	0.431(3)	0.936(5)	0.891(5)	6(1)[b]	0.5

Table 4-5. Continued.

Atom	x	y	z	B_{eq}	Occ
C(5)	0.646(2)	0.7500	0.673(2)	4.4(7)	0.5
C(6)	0.681(2)	0.7500	0.774(2)	6.7(10)	0.5
C(7)	0.561(2)	0.7500	0.408(2)	5.3(9)	0.5
C(8)	0.534(2)	0.7500	0.309(2)	6(1)	0.5
C(9)	0.320(3)	0.544(5)	0.519(4)	3.8(9)[b)]	0.5
C(10)	0.289(3)	0.548(4)	0.404(4)	4(1)[b)]	0.5
C(11)	0.335(7)	0.946(10)	0.525(8)	11.8(9)[b)]	0.5
C(12)	0.295(3)	0.955(5)	0.445(4)	5(1)[b)]	0.5
Br(1)	0.1036(2)	0.7500	0.4311(2)	5.49(9)	0.5
Br(2)	0.8418(3)	0.9273(3)	0.3495(2)	11.9(1)	
O(1w)	0.794(1)	0.7500	0.505(1)	7.7(8)	0.5

a) B_{eq} denotes the equivalent isotropic temperature factors, $B_{eq} = (8\pi^2/3)\Sigma\Sigma U_{ij}a^*_i a^*_j \boldsymbol{a}_i \cdot \boldsymbol{a}_j$
b) Refined isotropically.

Table 4-6. Final Atomic Coordinates, Equivalent Isotropic Thermal Parameters (B_{eq} / Å),[a)] and Occupancy Factors (Occ) for Non-Hydrogen Atoms of $[Mo_2O_3\{Rh(aet)_3\}_3]Br_4 \cdot 6H_2O$ ($7Br_4 \cdot 6H_2O$)

Atom	x	y	z	B_{eq}	Occ
Rh(1)	0.71927(5)	0.09434(5)	0.69502(6)	2.42(2)	
Rh(2)	0.77488(5)	0.66658(5)	1.08427(6)	2.19(1)	
Rh(3)	0.76639(5)	0.26954(5)	1.22537(6)	2.35(2)	
Mo(1)	0.80807(6)	0.24150(5)	0.91775(6)	2.32(2)	
Mo(2)	0.69642(6)	0.48135(6)	1.10355(6)	2.35(2)	
S(1)	0.6408(2)	0.1565(2)	0.8545(2)	2.74(5)	
S(2)	0.8547(2)	0.0607(2)	0.7888(2)	2.63(5)	
S(3)	0.7687(2)	0.2494(2)	0.7416(2)	3.24(6)	
S(4)	0.8666(2)	0.5187(2)	1.0511(2)	2.92(5)	
S(5)	0.7228(2)	0.6563(2)	1.2339(2)	3.09(5)	
S(6)	0.6539(2)	0.5737(2)	0.9828(2)	2.68(5)	
S(7)	0.8090(2)	0.1690(2)	1.0500(2)	2.49(5)	
S(8)	0.7863(2)	0.4250(2)	1.2324(2)	3.09(6)	
S(9)	0.6069(2)	0.2747(2)	1.1718(2)	3.43(6)	
O(1)	0.9172(5)	0.2792(5)	0.9433(5)	3.3(2)	
O(2)	0.5831(5)	0.4877(5)	1.1328(6)	3.7(2)	
O(3)	0.7288(4)	0.3555(4)	0.9962(5)	2.6(1)	

Table 4-6. Continued.

Atom	x	y	z	B_{eq}	Occ
N(1)	0.6699(6)	-0.0412(6)	0.6624(7)	3.4(2)	
N(2)	0.8011(6)	0.0317(6)	0.5568(6)	3.3(2)	
N(3)	0.6014(6)	0.1428(7)	0.6181(7)	3.8(2)	
N(4)	0.8289(6)	0.6637(5)	0.9466(6)	2.9(2)	
N(5)	0.8842(6)	0.7442(6)	1.1883(7)	3.8(2)	
N(6)	0.6797(6)	0.7929(6)	1.1062(6)	3.1(2)	
N(7)	0.9123(6)	0.2551(6)	1.2654(7)	3.5(2)	
N(8)	0.7317(6)	0.3505(6)	1.3888(6)	3.4(2)	
N(9)	0.7460(6)	0.1385(6)	1.2402(6)	3.0(2)	
C(1)	0.6369(8)	0.0360(7)	0.8559(9)	3.6(2)	
C(2)	0.6046(8)	-0.0361(8)	0.7450(9)	3.8(3)	
C(3)	0.9357(7)	0.0478(8)	0.6857(8)	3.6(2)	
C(4)	0.8929(7)	-0.0170(8)	0.5785(8)	3.5(2)	
C(5)	0.651(1)	0.3091(8)	0.7320(9)	5.1(3)	
C(6)	0.6050(10)	0.2435(10)	0.623(1)	5.6(4)	
C(7)	0.8794(7)	0.4888(7)	0.9084(8)	3.4(2)	
C(8)	0.9041(8)	0.5810(8)	0.8993(9)	3.7(2)	
C(9)	0.8386(9)	0.6775(8)	1.3130(9)	4.8(3)	
C(10)	0.8736(8)	0.7641(8)	1.3032(8)	4.1(3)	
C(11)	0.5585(7)	0.6737(8)	1.0414(9)	3.6(2)	
C(12)	0.5893(7)	0.7656(7)	1.0388(8)	3.2(2)	
C(13)	0.9331(7)	0.1410(8)	1.0769(9)	3.7(3)	
C(14)	0.9734(8)	0.2238(9)	1.170(1)	4.6(3)	
C(15)	0.728(1)	0.4993(8)	1.3597(9)	5.6(3)	
C(16)	0.751(1)	0.4526(10)	1.4344(9)	6.0(4)	
C(17)	0.583(1)	0.165(1)	1.185(1)	7.1(5)	
C(18)	0.647(1)	0.121(2)	1.227(2)	12.2(8)	
Br(1)	0.61980(9)	0.92823(10)	1.37811(9)	5.09(3)	
Br(2)	0.85476(10)	0.91668(8)	1.0865(1)	5.39(3)	
Br(3)	0.8847(1)	1.1873(1)	1.4728(1)	5.16(3)	
Br(4)	1.1942(1)	1.2643(1)	1.3785(1)	6.36(4)	
O(1w)	1.4473(8)	1.4557(9)	1.3251(9)	9.0(3)	
O(2w)	1.5261(9)	1.3768(10)	1.479(1)	9.6(3)	
O(3w)	1.2594(10)	1.425(1)	1.281(1)	10.4(4)	
O(4w)	1.104(1)	1.586(1)	1.356(1)	8.8(4)	0.7
O(5w)	1.396(1)	1.255(1)	1.504(1)	8.3(4)	0.7
O(6w)	1.288(1)	1.178(1)	1.127(2)	8.4(5)	0.6
O(7w)	1.021(2)	0.439(2)	0.415(2)	14.6(8)	0.6
O(8w)	1.001(2)	0.402(2)	0.492(2)	6.4(5)	0.4

a) B_{eq} denotes the equivalent isotropic temperature factors, $B_{eq} = (8\pi^2/3)\Sigma\Sigma U_{ij}a^*_i a^*_j \boldsymbol{a}_i \cdot \boldsymbol{a}_j$

Table 4-7. Final Atomic Coordinates, Equivalent Isotropic Thermal Parameters (B_{eq} / Å),[a] and Occupancy Factors (Occ) for Non-Hydrogen Atoms of $[Fe\{Rh(aet)_3\}_2](NO_3)_3 \cdot 4H_2O$ ($9(NO_3)_3 \cdot 4H_2O$)

Atom	x	y	z	B_{eq}	Occ
Rh(1)	0.85755(5)	0.22958(4)	0.22156(5)	2.47(1)	
Fe(1)	1.0000	0.0000	0.0000	2.37(2)	0.5
S(1)	0.7556(2)	0.1361(1)	-0.0376(2)	2.81(3)	
S(2)	1.0940(2)	0.1727(1)	0.1137(2)	2.80(3)	
S(3)	0.9444(2)	0.0352(1)	0.2570(2)	2.71(3)	
N(1)	0.6326(7)	0.2624(5)	0.2885(7)	3.7(1)	
N(2)	0.8033(7)	0.3979(5)	0.1689(7)	3.5(1)	
N(3)	0.9699(7)	0.2924(5)	0.4609(6)	3.3(1)	
C(1)	0.5951(8)	0.1081(7)	0.0281(9)	3.7(1)	
C(2)	0.517(1)	0.2238(8)	0.150(1)	4.7(2)	
C(3)	1.0261(9)	0.2869(6)	0.0025(8)	3.4(1)	
C(4)	0.942(1)	0.4087(7)	0.115(1)	4.2(2)	
C(5)	1.1086(9)	0.0701(7)	0.4145(8)	3.6(1)	
C(6)	1.0427(9)	0.1914(7)	0.5366(8)	3.9(2)	
N(4)	0.6570(10)	0.4445(9)	-0.2582(10)	5.5(2)	
N(5)	0.518(2)	0.087(3)	-0.512(3)	7.7(5)	0.5
O(1)	0.780(2)	0.401(3)	-0.262(2)	26.8(9)	
O(2)	0.578(1)	0.4631(9)	-0.154(1)	8.8(3)	
O(3)	0.608(3)	0.482(1)	-0.367(2)	16.7(6)	
O(4)	0.535(2)	0.194(1)	-0.458(2)	7.0(4)	0.5
O(5)	0.536(2)	-0.029(2)	-0.610(2)	22.3(6)	
O(1w)	0.366(2)	0.303(2)	-0.202(3)	21.3(9)	
O(2w)	0.2441(7)	0.4005(6)	-0.4936(8)	5.2(1)	

a) B_{eq} denotes the equivalent isotropic temperature factors, $B_{eq} = (8\pi^2/3)\Sigma\Sigma U_{ij} a^*_i a^*_j a_i \cdot a_j$

Table 4-8. Final Atomic Coordinates, Equivalent Isotropic Thermal Parameters (B_{eq} / Å),[a] and Occupancy Factors (Occ) for Non-Hydrogen Atoms of $[Co\{Rh(aet)_3\}_2](NO_3)_3 \cdot 3H_2O$ ($10(NO_3)_3 \cdot 3H_2O$)

Atom	x	y	z	B_{eq}	Occ
Rh(1)	0.85456(6)	0.23318(4)	0.22565(5)	2.55(2)	
Co(1)	1.0000	0.0000	0.0000	2.41(3)	0.5
S(1)	1.0885(2)	0.1734(1)	0.1156(2)	2.74(4)	
S(2)	0.9426(2)	0.0378(2)	0.2554(2)	2.89(4)	
S(3)	0.7581(2)	0.1366(2)	-0.0341(2)	2.96(4)	
N(1)	0.8032(8)	0.4006(5)	0.1690(7)	3.3(1)	
N(2)	0.9697(8)	0.2936(5)	0.4662(7)	3.6(1)	
N(3)	0.6290(8)	0.2634(5)	0.2893(7)	3.9(2)	
C(1)	1.0222(10)	0.2874(7)	0.0013(9)	3.6(2)	
C(2)	0.939(1)	0.4072(6)	0.1120(10)	4.4(2)	
C(3)	1.1073(10)	0.0682(7)	0.4124(9)	3.8(2)	
C(4)	1.045(1)	0.1900(7)	0.5375(9)	4.0(2)	
C(5)	0.6015(9)	0.1040(7)	0.0253(9)	3.7(2)	
C(6)	0.516(1)	0.2216(8)	0.147(1)	4.6(2)	
N(4)	0.657(1)	0.4444(9)	0.7406(9)	5.8(2)	
N(5)	0.524(3)	0.102(3)	0.502(2)	8.5(7)	0.5
O(1)	0.579(1)	0.4629(8)	0.847(1)	8.2(2)	
O(2)	0.733(3)	0.487(2)	0.703(3)	9.9(5)	0.5
O(3)	0.797(2)	0.415(2)	0.757(2)	7.8(4)	0.5
O(4)	0.581(2)	0.484(1)	0.616(1)	5.2(2)	0.5
O(5)	0.718(3)	0.317(2)	0.678(3)	10.5(5)	0.5
O(6)	0.526(2)	0.196(1)	0.542(2)	7.7(5)	0.5
O(7)	0.535(3)	0.026(3)	0.379(5)	12(1)	0.5
O(8)	0.478(2)	0.050(2)	0.606(2)	7.3(5)	0.5
O(1w)	0.2435(7)	0.3999(5)	0.5076(7)	5.0(1)	
O(2w)	0.364(2)	0.303(2)	0.809(3)	9.9(6)	0.5

a) B_{eq} denotes the equivalent isotropic temperature factors, $B_{eq} = (8\pi^2/3)\Sigma\Sigma U_{ij} a^*_i a^*_j \boldsymbol{a}_i \cdot \boldsymbol{a}_j$

4-3. Results and Discussion

4-3-1. X-Ray Crystal Structures

X-Ray structural analysis of $5Br_4 \cdot 4H_2O$ or $6Br_3 \cdot H_2O$ revealed the presence of a discrete complex cation, bromide anions, and water molecules. The perspective drawings of the entire complex cations **5** and **6** are given in Figures 4-1 and 4-2, respectively. The selected bond distances and angles are listed in Tables 4-9 and 4-10. Both the complex cations **5** and **6** consist of two approximately octahedral *fac(S)*-$[M(aet)_3]$ ($M = Ir^{III}$ (**5**), Rh^{III} (**6**)) units and one molybdenum atom. These are consistent with the plasma emission spectral analysis, which gave a value of Mo : M = 1 : 2. The three thiolato sulfur atoms in each *fac(S)*-$[M(aet)_3]$ unit coordinate to the central molybdenum atom. These indicate, therefore, that **5** and **6** complete linear-type S-bridged trinuclear structures, which molybdenum ion was incorporated at a center. However, it is noticed that the valence of the molybdenum ion is different from between **5** and **6**. The total number of bromide anions implies that the entire complex cation **5** is tetravalent, while the entire complex cation **6** is trivalent. These are supported by their elemental analyses. The difference of the valence would be due to the difference of electrochemical properties between *fac(S)*-$[Ir(aet)_3]$ and *fac(S)*-$[Rh(aet)_3]$ (vide infra).

As shown in Figure 4-1, the complex cation **5** form a linear-type S-bridged $Ir^{III}Mo^{IV}Ir^{III}$ trinuclear structure. The crystallographic inversion center locates on the central molybdenum atom and it requires that the three metals are aligned to be exactly linear with the two identical Ir-Mo distances. In this structure, the molybdenum atom is situated in a $Mo^{IV}S_6$ octahedral environment. The overall structure of **5** is similar to that of the previously reported S-bridged trinuclear complexes.[10,19,20] It is noted that the Ir-Mo distances (2.7469(7) Å) in **5** are extremely shorter than the corresponding Ir-Cr ones (2.9096(3) Å) in $\Delta\Lambda$-$[Cr\{Ir(aet)_3\}_2]^{3+}$ (**1a**), although the Mo-S distances (average 2.458(7) Å) are longer than the corresponding Cr-S ones (average 2.421(2) Å). The bridging Ir-S-Mo bite angles (average 69.8(2) °) are acute, compared with the corresponding Ir-S-Cr ones (average 75.51(5) °).

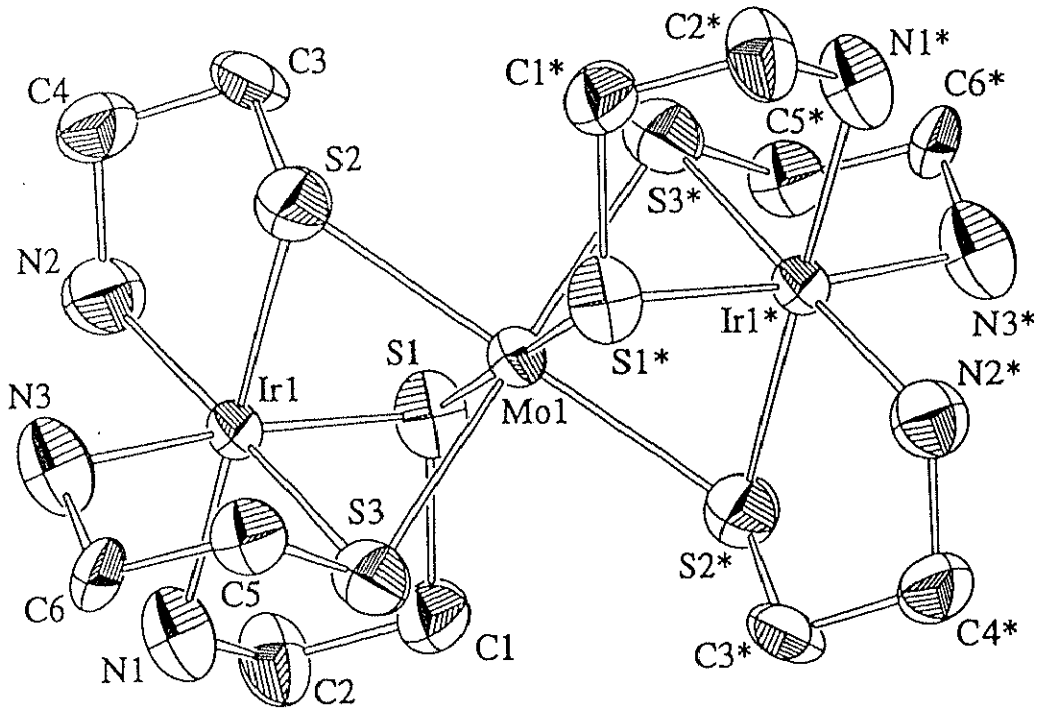

Figure 4-1. Perspective view of $\Delta\Lambda$-$[Mo\{Ir(aet)_3\}_2]^{4+}$ (5) with the atomic labeling scheme.

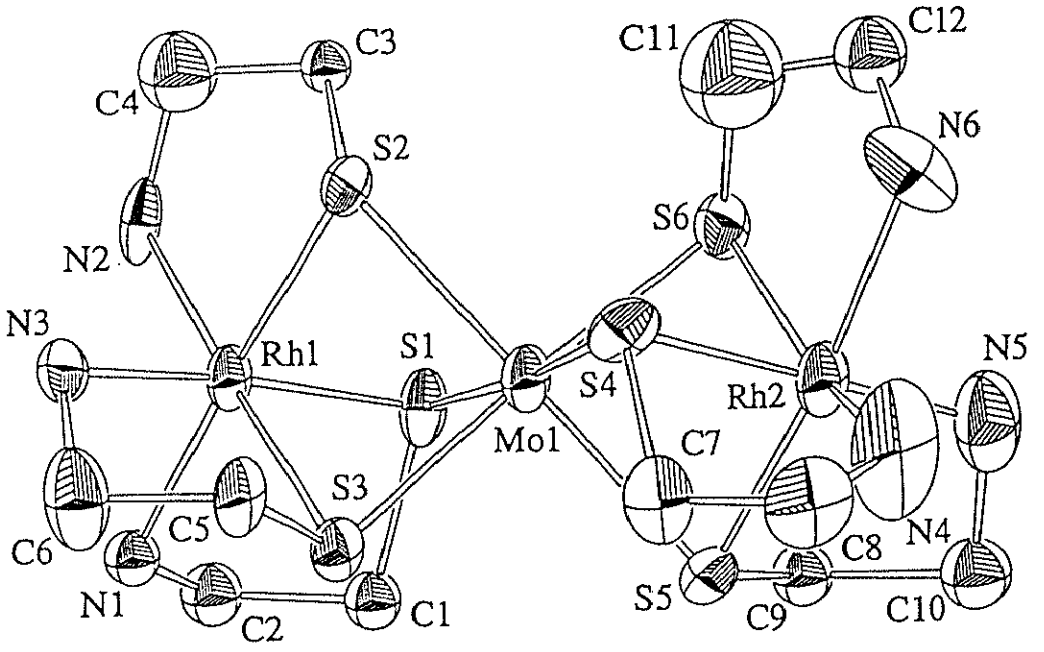

Figure 4-2. Perspective view of $\Delta\Delta$-$[Mo\{Rh(aet)_3\}_2]^{3+}$ (6) with the atomic labeling scheme. The overlapped $\Lambda\Lambda$ isomer is omitted for clarity.

Table 4-9. Selected Bond Distances (Å) and Angles (°) for $[Mo\{Ir(aet)_3\}_2]^{4+}$ (5)

Ir(1)-Mo(1)	2.7469(7)				
Ir(1)-S(1)	2.340(7)	Ir(1)-N(1)	2.11(2)	Mo(1)-S(1)	2.455(7)
Ir(1)-S(2)	2.332(6)	Ir(1)-N(2)	2.08(2)	Mo(1)-S(2)	2.456(6)
Ir(1)-S(3)	2.352(7)	Ir(1)-N(3)	2.11(2)	Mo(1)-S(3)	2.463(6)

S(1)-Ir(1)-S(2)	94.5(2)	S(1)-Mo(1)-S(2)	88.6(2)
S(1)-Ir(1)-S(3)	92.4(2)	S(1)-Mo(1)-S(3)	87.0(2)
S(2)-Ir(1)-S(3)	93.0(2)	S(2)-Mo(1)-S(3)	87.4(2)
N(1)-Ir(1)-N(2)	93.9(8)	Ir(1)-S(1)-Mo(1)	69.9(2)
N(1)-Ir(1)-N(3)	89.8(8)	Ir(1)-S(2)-Mo(1)	70.0(2)
N(2)-Ir(1)-N(3)	92.5(9)	Ir(1)-S(3)-Mo(1)	69.5(2)

Table 4-10. Selected Bond Distances (Å) and Angles (°) for $[Mo\{Rh(aet)_3\}_2]^{3+}$ (6)

Rh(1)-Mo(1)	2.852(3)	Rh(2)-Mo(1)	2.868(3)		
Rh(1)-S(1)	2.365(10)	Rh(2)-S(4)	2.41(1)	Mo(1)-S(1)	2.438(9)
Rh(1)-S(2)	2.283(9)	Rh(2)-S(5)	2.22(1)	Mo(1)-S(2)	2.434(9)
Rh(1)-S(3)	2.347(9)	Rh(2)-S(6)	2.359(10)	Mo(1)-S(3)	2.432(10)
Rh(1)-N(1)	2.17(3)	Rh(2)-N(4)	2.04(3)	Mo(1)-S(4)	2.43(1)
Rh(1)-N(2)	2.05(3)	Rh(2)-N(5)	2.04(4)	Mo(1)-S(5)	2.474(10)
Rh(1)-N(3)	2.02(3)	Rh(2)-N(6)	2.19(4)	Mo(1)-S(6)	2.43(1)

S(1)-Rh(1)-S(2)	91.0(4)	S(1)-Mo(1)-S(2)	85.7(3)
S(1)-Rh(1)-S(3)	88.1(3)	S(1)-Mo(1)-S(3)	84.6(3)
S(2)-Rh(1)-S(3)	91.7(3)	S(2)-Mo(1)-S(3)	86.1(3)
N(1)-Rh(1)-N(2)	93(1)	S(4)-Mo(1)-S(5)	83.8(4)
N(1)-Rh(1)-N(3)	92(1)	S(4)-Mo(1)-S(6)	87.3(4)
N(2)-Rh(1)-N(3)	93(1)	S(5)-Mo(1)-S(6)	84.0(3)
S(4)-Rh(2)-S(5)	90.0(4)	Rh(1)-S(1)-Mo(1)	72.8(3)
S(4)-Rh(2)-S(6)	89.5(3)	Rh(1)-S(2)-Mo(1)	74.3(3)
S(5)-Rh(2)-S(6)	91.4(4)	Rh(1)-S(3)-Mo(1)	73.3(3)
N(4)-Rh(2)-N(5)	103(1)	Rh(2)-S(4)-Mo(1)	72.7(3)
N(4)-Rh(2)-N(6)	81.8(9)	Rh(2)-S(5)-Mo(1)	75.0(3)
N(5)-Rh(2)-N(6)	95(1)	Rh(2)-S(6)-Mo(1)	73.6(3)

The metal-metal distances of **5** are the shortest in those of the reported S-bridged trinuclear structures. Considering the absolute configurations (Δ and

Λ) of the two terminal *fac(S)*-[Ir(aet)$_3$] units, three isomers ($\Delta\Delta$, $\Lambda\Lambda$, and $\Delta\Lambda$) are possible for the [Mo{Ir(aet)$_3$}$_2$]$^{3+}$. Crystal 5 consists of the $\Delta\Lambda$ isomer. This stereochemical behavior, which involves configuration of the bridging sulfur atoms, is wholly consistent with that observed in $\Delta\Lambda$-[Cr^{III}{M(aet)$_3$}$_2$]$^{3+}$ (**1a**).

As shown in Figure 4-2, the complex cation 6 form a linear-type S-bridged Rh^{III}Mo^{III}Rh^{III} trinuclear structure. In this structure, the molybdenum atom is situated in a Mo^{III}S$_6$ octahedral environment. The overall structure of 6 is similar to that of 5. The Rh-Mo distances (average 2.860(3) Å) in 6 are shorter than the corresponding Rh-Cr ones (2.9328(2) Å) in $\Delta\Lambda$-[Cr{Rh(aet)$_3$}$_2$]$^{3+}$ (**2a**). The bridging Rh-S-Mo bite angles (average 73.6(3) °) are acute, compared with the corresponding Rh-S-Cr ones (average 76.53(2) °). Considering the absolute configurations (Δ and Λ) of the two terminal *fac(S)*-[Rh(aet)$_3$] units, crystal **6** consists of the $\Delta\Delta$ and $\Lambda\Lambda$ isomers, which combine to form the racemic compound. This stereochemical behavior, which involves configuration of the bridging sulfur atoms, is wholly consistent with that observed in $\Delta\Delta/\Lambda\Lambda$-[Ni{Rh(aet)$_3$}$_2$]$^{2+}$.[19] The two *fac(S)*-[Rh(aet)$_3$] units in 6 have the same chiral configuration to form the $\Delta\Delta$ and $\Lambda\Lambda$ isomers; the former isomer is illustrated in Figure 4-2. In the unit cell, the $\Delta\Delta$ and $\Lambda\Lambda$ isomers co-exist in each of four sites with a site occupancy of 0.5, which indicates that crystal **6** is not a racemic compound but a rare example of a solid solution.[21]

X-Ray structural analysis of 7Br$_4$·6H$_2$O revealed the presence of a discrete complex cation, bromide anions, and water molecules. The perspective drawing of the entire complex cation 7 is given in Figure 4-3. The selected bond distances and angles are listed in Table 4-11. As shown in Figure 4-3, the complex cation 7 consists of three approximately octahedral *fac(S)*-[Rh(aet)$_3$] units, retaining the structure of the starting mononuclear complex, and oxomolybdenum dinuclear unit, bridged by an oxygen atom. This is consistent with the plasma emission spectral analysis which gave a value of Mo : Rh = 2 : 3. Two molybdenum atoms are bridged by one oxygen atom to form a Mo$_2$O$_2$(μ-O)$^{4+}$ moiety, in which O(1) and O(2) atoms are anti position each other. Each Rh(1) and Rh(2) unit bound to one

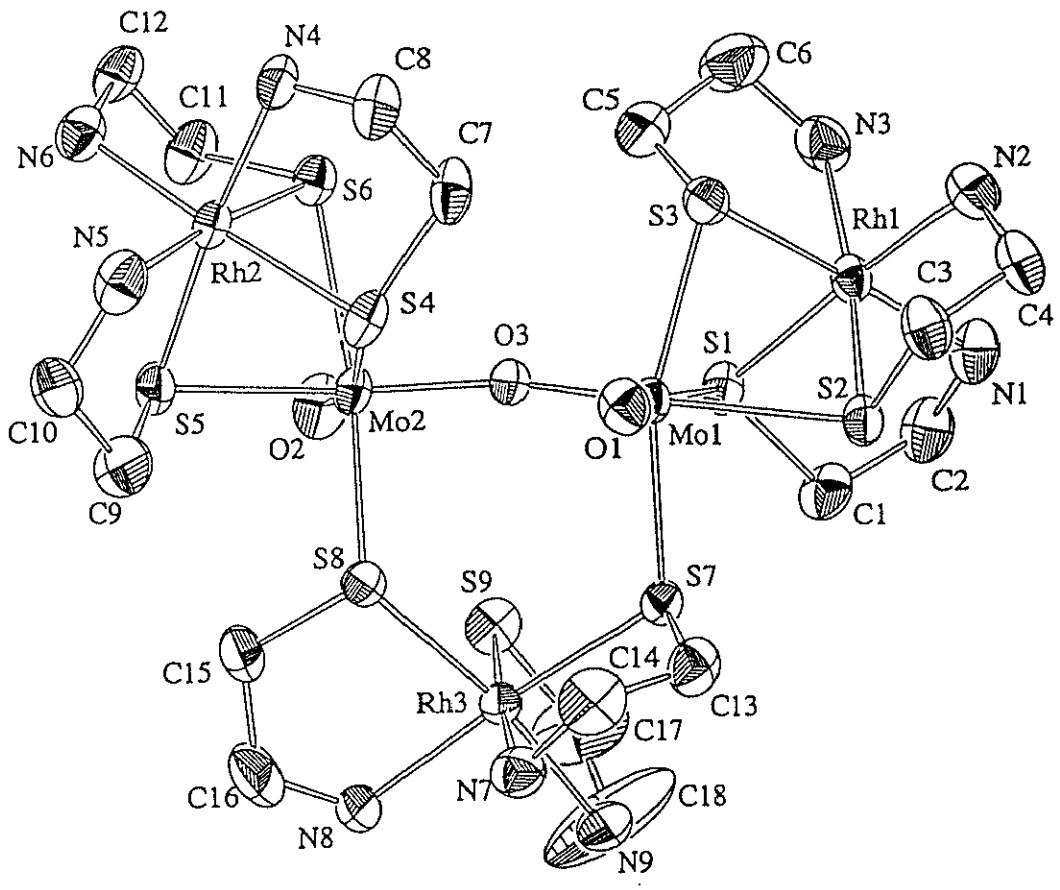

Figure 4-3. Perspective view of $\Delta\Lambda\Lambda$-$[Mo_2O_3\{Rh(aet)_3\}_3]^{4+}$ (7) with the atomic labeling scheme.

molybdenum atom, while Rh(3) unit bridges between two molybdenum atoms, remaining S(9) atom as a non-bridging thiolato atom. That is, eight sulfur atoms (S(1) - S(8)) are bridging thiolato atoms, linking between Rh^{III} and Mo^{V}, and to form a novel $Rh^{III}_3Mo^{V}_2$ pentanuclear structure. In this structure, two molybdenum atoms are situated in considerably distorted $Mo^{V}O_2S_4$ octahedral environments, and all metal atoms are nonequivalent. The bond distances and angles in Rh(1) and Rh(2) units are within the approximate ranges observed for the previous reported *fac(S)*-$[Rh(aet)_3]$ unit, whose three thiolato sulfur atoms coordinate to the same metal.[10,19,20,22] However, Rh(3) unit is distorted from regular one. In particular, S(7)-Rh(3)-S(8) angle (100.24(9) °) is significantly deviated from 90 °, which bridging between two molybdenum atoms, resulting in the formation of six-membered ring. This is much larger

Table 4-11. Selected Bond Distances (Å) and Angles (°) for $[Mo_2O_3\{Rh(aet)_3\}_3]^{4+}$ (7)

Rh(1)-Mo(1)	3.165(1)	Rh(2)-Mo(2)	3.229(1)		
Rh(3)-Mo(1)	4.127(1)	Rh(3)-Mo(2)	4.121(1)	Mo(1)-Mo(2)	3.664(1)
Rh(1)-S(1)	2.310(3)	Rh(2)-S(4)	2.302(2)	Rh(3)-S(7)	2.315(2)
Rh(1)-S(2)	2.324(3)	Rh(2)-S(5)	2.306(3)	Rh(3)-S(8)	2.334(3)
Rh(1)-S(3)	2.315(2)	Rh(2)-S(6)	2.313(3)	Rh(3)-S(9)	2.318(3)
Rh(1)-N(1)	2.083(8)	Rh(2)-N(4)	2.078(8)	Rh(3)-N(7)	2.102(9)
Rh(1)-N(2)	2.107(8)	Rh(2)-N(5)	2.107(8)	Rh(3)-N(8)	2.112(8)
Rh(1)-N(3)	2.100(9)	Rh(2)-N(6)	2.101(8)	Rh(3)-N(9)	2.107(8)
Mo(1)-S(1)	2.738(3)	Mo(2)-S(4)	2.778(3)	Mo(1)-O(1)	1.671(7)
Mo(1)-S(2)	2.565(2)	Mo(2)-S(5)	2.518(2)	Mo(1)-O(3)	1.875(6)
Mo(1)-S(3)	2.459(3)	Mo(2)-S(6)	2.541(3)	Mo(2)-O(2)	1.681(7)
Mo(1)-S(7)	2.458(2)	Mo(2)-S(8)	2.439(3)	Mo(2)-O(3)	1.864(6)

S(1)-Rh(1)-S(2)	88.34(9)	S(1)-Mo(1)-S(2)	74.93(8)
S(1)-Rh(1)-S(3)	89.47(9)	S(1)-Mo(1)-S(3)	77.34(8)
S(2)-Rh(1)-S(3)	87.50(9)	S(2)-Mo(1)-S(3)	79.35(8)
N(1)-Rh(1)-N(2)	92.2(3)	S(7)-Mo(1)-O(1)	100.1(2)
N(1)-Rh(1)-N(3)	94.4(3)	S(7)-Mo(1)-O(3)	94.6(2)
N(2)-Rh(1)-N(3)	94.8(3)	O(1)-Mo(1)-O(3)	104.5(3)
S(4)-Rh(2)-S(5)	87.81(9)	O(1)-Mo(1)-S(1)	172.1(2)
S(4)-Rh(2)-S(6)	87.29(9)	O(1)-Mo(1)-S(2)	97.3(2)
S(5)-Rh(2)-S(6)	88.06(9)	O(1)-Mo(1)-S(3)	100.2(2)
N(4)-Rh(2)-N(5)	93.8(3)	S(4)-Mo(2)-S(5)	74.02(8)
N(4)-Rh(2)-N(6)	93.5(3)	S(4)-Mo(2)-S(6)	73.42(8)
N(5)-Rh(2)-N(6)	95.8(3)	S(5)-Mo(2)-S(6)	78.77(8)
S(7)-Rh(3)-S(8)	100.24(9)	S(8)-Mo(2)-O(2)	103.5(3)
S(7)-Rh(3)-S(9)	91.73(9)	S(8)-Mo(2)-O(3)	87.4(2)
S(8)-Rh(3)-S(9)	95.04(10)	O(2)-Mo(2)-O(3)	108.1(3)
N(7)-Rh(3)-N(8)	92.9(3)	O(2)-Mo(2)-S(4)	164.6(2)
N(7)-Rh(3)-N(9)	92.0(3)	O(2)-Mo(2)-S(5)	96.0(2)
N(8)-Rh(3)-N(9)	88.6(3)	O(2)-Mo(2)-S(6)	93.3(3)
Rh(1)-S(1)-Mo(1)	77.14(7)	Rh(2)-S(4)-Mo(2)	78.32(8)
Rh(1)-S(2)-Mo(1)	80.52(8)	Rh(2)-S(5)-Mo(2)	83.92(8)
Rh(1)-S(3)-Mo(1)	83.01(8)	Rh(2)-S(6)-Mo(2)	83.26(8)
Rh(3)-S(7)-Mo(1)	119.68(10)	Rh(3)-S(8)-Mo(2)	119.4(1)
Mo(1)-O(3)-Mo(2)	157.0(4)		

than that in *fac(S)*-$[Rh(aet)_3]$ unit, whose three thiolato sulfur atoms coordinate to different metals.[21-23] Corresponding N(8)-Rh(3)-N(9) angle (88.6(3) °) is acuter than other N-Rh-N ones. Mo(1)-O(1) and Mo(2)-O(2)

distances (average 1.676(7) Å) imply double bonds and Mo(1)-O(3) and Mo(2)-O(3) distances (average 1.870(6) Å) indicate single bonds. For Mo-S distances, the Mo-S bond distances *trans* to the Mo-O double bonds (average 2.758(3) Å) are significantly longer than the others (average 2.497(3) Å). It can be considered due to trans influence, and similar lengthening was also observed for dinuclear molybdenum complexes.[6] The Mo(1)-Rh(1) and Mo(2)-Rh(2) distances (3.165(1) and 3.229(1) Å, respectively) are relatively longer because of long Mo-S distances (average 2.587(3) and 2.612(3) Å, respectively) and acute S-Mo-S angles (average 77.21(8) and 75.40(8) °, respectively). In fact, Mo(1)-S-Rh(3) and Mo(2)-S-Rh(2) angles (average 80.22(8) and 81.83(8) °, respectively) in **7** are larger than those in **6**. The Mo-Mo distances (3.664(1) Å) in **7** is longer than those of the complexes which containing $Mo_2O_4^{2+}$ unit.[24] The Mo-O-Mo angles in the most complexes containing $Mo_2O_3^{4+}$ unit are close to 180 °.[6] However, Mo-O-Mo angle (157.0(4) °) in **7** is unique as that in tetranuclear Mo complex, $[Mo_4O_{12}(C_8H_6N_4)]^{2-}$ (average 141.8(7) °).[25] Considering the absolute configurations, crystal **7** consists of a pair of enantiomers, Δ(Rh1)Λ(Rh2)Λ(Rh3) and Λ(Rh1)Δ(Rh2)Δ(Rh3); the latter isomer is illustrated in Figure 4-3. All the bridging sulfur atoms are fixed to the *R* configuration for the Δ unit and the *S* configuration for the Λ unit.

X-Ray structural analysis of $\mathbf{9}(NO_3)_3\cdot 4H_2O$ or $\mathbf{10}(NO_3)_3\cdot 3H_2O$ revealed the presence of discrete trivalent complex cation, nitrate anions, and water molecules. The perspective drawing of the entire complex cations **9** and **10** are given in Figures 4-4 and 4-5, respectively. The selected bond distances and angles for these complexes are listed in Table 4-12. The complex cations are isostructural with the complex cations **1a** and **2a**, consisting of two approximately octahedral *fac(S)*-[$Rh(aet)_3$] units and one iron or cobalt atom (Figures 4-4 and 4-5). Namely, the three thiolato sulfur atoms in each *fac(S)*-[$Rh(aet)_3$] unit coordinate to the central iron or cobalt atom, forming linear-type S-bridged $Rh^{III}M'Rh^{III}$ trinuclear structures, $[M'\{Rh(aet)_3\}_2]^{3+}$ which containing the $M'S_6$ chromophore (M' = Fe^{III} and Co^{III}). The absolute configurations and conformations of the complexes **9** and **10** are wholly consistent with **1a** and **2a** (see Figures 2-1, 2-2, 4-4, and 4-5).

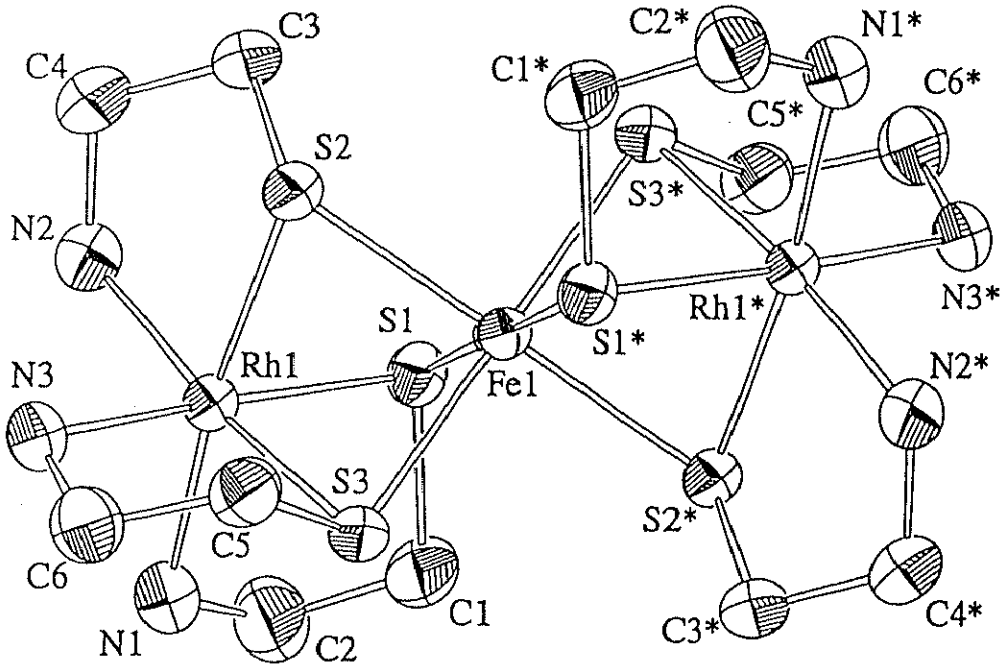

Figure 4-4. Perspective view of $\Delta\Lambda$-$[Fe\{Rh(aet)_3\}_2]^{3+}$ (**9**) with the atomic labeling scheme.

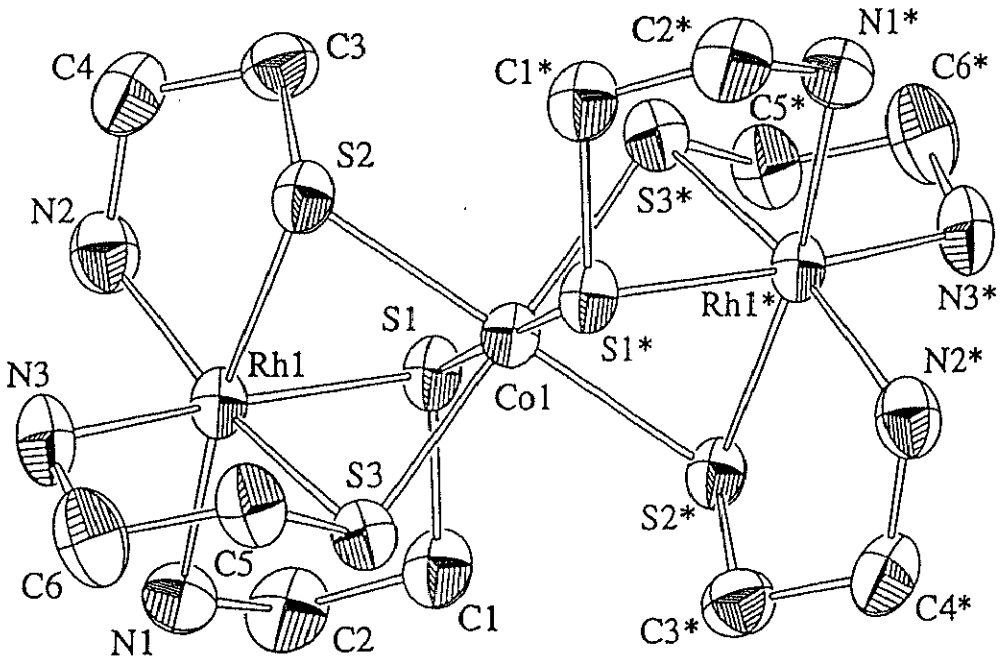

Figure 4-5. Perspective view of $\Delta\Lambda$-$[Co\{Rh(aet)_3\}_2]^{3+}$ (**10**) with the atomic labeling scheme.

Table 4-12. Selected Bond Distances (Å) and Angles (°) for $[Fe\{Rh(aet)_3\}_2]^{3+}$ and $[Co\{Rh(aet)_3\}_2]^{3+}$

$[Fe\{Rh(aet)_3\}_2]^{3+}$ (9)		$[Co\{Rh(aet)_3\}_2]^{3+}$ (10)	
Rh(1)-Fe(1)	2.8411(4)	Rh(1)-Co(1)	2.9098(5)
Rh(1)-S(1)	2.309(2)	Rh(1)-S(1)	2.305(2)
Rh(1)-S(2)	2.313(2)	Rh(1)-S(2)	2.311(2)
Rh(1)-S(3)	2.318(2)	Rh(1)-S(3)	2.305(2)
Rh(1)-N(1)	2.101(6)	Rh(1)-N(1)	2.124(5)
Rh(1)-N(2)	2.112(6)	Rh(1)-N(2)	2.137(6)
Rh(1)-N(3)	2.129(5)	Rh(1)-N(3)	2.105(7)
Fe(1)-S(1)	2.298(2)	Co(1)-S(1)	2.301(2)
Fe(1)-S(2)	2.317(1)	Co(1)-S(2)	2.288(2)
Fe(1)-S(3)	2.303(1)	Co(1)-S(3)	2.283(2)
S(1)-Rh(1)-S(2)	85.84(5)	S(1)-Rh(1)-S(2)	83.44(6)
S(1)-Rh(1)-S(3)	86.68(5)	S(1)-Rh(1)-S(3)	83.62(7)
S(2)-Rh(1)-S(3)	85.36(6)	S(2)-Rh(1)-S(3)	84.45(6)
N(1)-Rh(1)-N(2)	95.4(2)	N(1)-Rh(1)-N(2)	96.6(2)
N(1)-Rh(1)-N(3)	96.3(2)	N(1)-Rh(1)-N(3)	96.6(2)
N(2)-Rh(1)-N(3)	95.7(2)	N(2)-Rh(1)-N(3)	97.2(2)
S(1)-Fe(1)-S(2)	86.01(5)	S(1)-Co(1)-S(2)	84.04(6)
S(1)-Fe(1)-S(3)	87.29(5)	S(1)-Co(1)-S(3)	84.22(6)
S(2)-Fe(1)-S(3)	85.61(5)	S(2)-Co(1)-S(3)	85.47(7)
Rh(1)-S(1)-Fe(1)	76.16(5)	Rh(1)-S(1)-Co(1)	78.37(6)
Rh(1)-S(2)-Fe(1)	75.69(4)	Rh(1)-S(2)-Co(1)	78.50(5)
Rh(1)-S(3)-Fe(1)	75.87(4)	Rh(1)-S(3)-Co(1)	78.72(6)

4-3-2. Characterization

The electronic absorption spectra of **5**, **6**, and **7** are shown in Figure 4-6. The ε values of the absorption spectrum of **7** were halved by considering the number of molybdenum in the complex. The diffuse reflectance as well as absorption spectral data are summarized in Table 4-13. The most intense band (ca. 50 x 10^3 cm^{-1}) in the UV region for **5** corresponds well to the sulfur-to-iridium charge transfer band as observed in the complexes involving *fac(S)*-$[Ir(aet)_3]$ units.[20] Quite similarly, the most intense band (ca. 45 x 10^3 cm^{-1}) in the UV region for **6** and **7** corresponds well to the sulfur-to-rhodium charge transfer band as observed in the complexes involving *fac(S)*-$[Rh(aet)_3]$ units.[12]

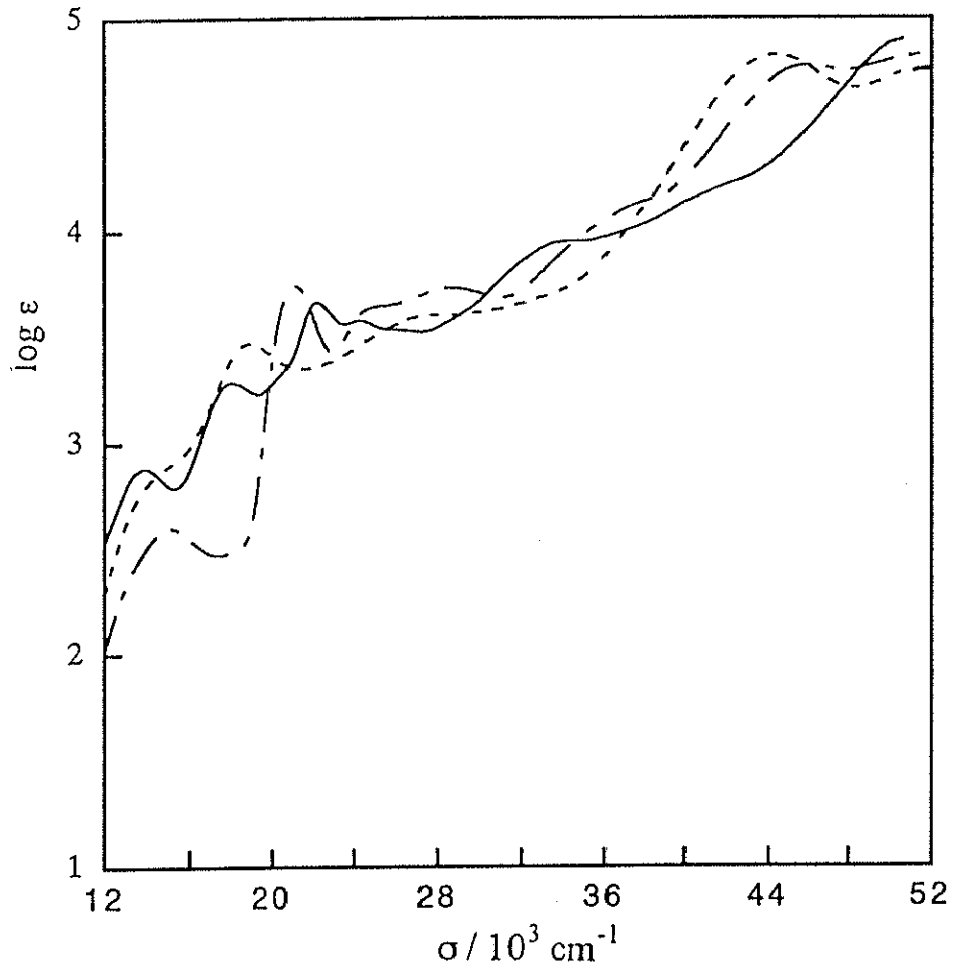

Figure 4-6. Electronic absorption spectra of $[Mo\{Ir(aet)_3\}_2]^{4+}$ (**5**; ————), $[Mo\{Rh(aet)_3\}_2]^{3+}$ (**6**; — · —), and $[Mo_2O_3\{Rh(aet)_3\}_3]^{4+}$ (**7**; – – – –).

The characteristic intense bands in the visible region are assigned as arising from the central $M'S_6$ ($M' = Cr^{III}$, Co^{III}, and Ni^{II}) chromophore, taking account of the absorption spectral behavior of the *fac(S)*-$[M(aet)_3]$ ($M = Ir^{III}$ and Rh^{III}) units in the corresponding region (chapter 2).[10] Therefore, it is assumed that the characteristic intense bands in the visible region are assigned as arising from the central $Mo^{IV}S_6$, $Mo^{III}S_6$, or $Mo^{V}_2O_3S_8$ chromophore. The absorption spectra of $[(Ph_3P)Cu(\mu\text{-}SR)_3Mo^{IV}(\mu\text{-}SR)_3Cu(Ph_3P)]$, which involve a $Mo^{IV}S_6$ chromophore, have some characteristic band in the visible region.[7] The intense visible bands at 22.22 and 24.27 x 10^3 cm^{-1} for **5** coincide well with the intense bands at 21.32 - 21.69 and 23.92 - 24.39 x 10^3 cm^{-1} (469 - 461 and 418 - 410 nm) for the copper complexes, respectively. However, the intense

Table 4-13. Electronic Absorption and Diffuse Reflectance Spectral Data of $[Mo\{Ir(aet)_3\}_2]^{4+}$, $[Mo\{Rh(aet)_3\}_2]^{3+}$, $[Mo_2O_3\{Rh(aet)_3\}_3]^{4+}$, and $[Mo_2O_4\{Co(aet)_3\}_2]^{2+}$

Complexes	Absorption maxima σ / 10^3 cm^{-1} (log ε / mol^{-1} dm^3 cm^{-1})	Reflectance maxima σ / 10^3 cm^{-1}
$[Mo\{Ir(aet)_3\}_2]^{4+}$ (5)	13.91 (2.88) 18.03 (3.29) 22.22 (3.66) 24.27 (3.58) 34.5 (3.9sh[a]) 41.0 (4.2sh)	14.2 17.7 22.4 24.0sh
$[Mo\{Rh(aet)_3\}_2]^{3+}$ (6)	15.04 (2.60) 21.16 (3.74) 24.97 (3.64) 28.57 (3.73) 37.2 (4.1sh) 45.9 (4.8sh)	20.9 24.8sh 27.8
$[Mo_2O_3\{Rh(aet)_3\}_3]^{4+}$ (7)	15.1 (3.2sh) 18.90 (3.77) 28.3 (3.9sh) 44.25 (5.13)	18.6 21.2 25.0sh
$[Mo_2O_4\{Co(aet)_3\}_2]^{2+}$ (8)	19.0 (3.0sh) 23.6 (3.0sh) 27.2 (3.8sh) 31.5 (4.2sh) 35.64 (4.49) 38.9 (4.4sh) 51.02 (4.71)	18.6 23.4sh 27.0sh 32.3sh

a) sh denotes a shoulder.

bands at lower energy region for **5** do not similar to those for the copper complexes. Namely, the intense bands at lower energy region imply the interaction between central molybdenum and terminal metals. This difference of spectral pattern would be due to the difference of terminal metal ions. Additionally, the absorption spectral pattern in lower energy region of **6** does not similar to that of corresponding chromium(III) complex **2b** in spite of involving d^3 type metal ion. Absorption spectral bands for **5** and **6** in

water are observed at similar position to the bands of diffuse reflectance spectra (Table 4-13). This indicates that **5** and **6** retain the trinuclear structure in solution.

Table 4-14. Infrared and Raman Spectral Data of $[M_2(aet)_4(cysta)]^{2+}$ and Its Related Complexes

Complexes	peak σ / cm^{-1}
$[Mo\{Ir(aet)_3\}_2]^{4+}$ (**5**)	
Infrared spectra	3436s 3142vs 3019vs 1615w 1587s 1450w 1419m 1387w 1318m 1268m 1233w 1167m 1115w 1032w 983m 918w 843w 759w 652w 524w
$[Mo\{Rh(aet)_3\}_2]^{3+}$ (**6**)	
Infrared spectra	3391s 3172vs 3083vs 2945w 2910w 1646w 1579s 1448m 1418m 1377w 1307w 1265m 1227w 1142m 1098w 1034w 977m 916w 840w 740w 644w 525w 419w
$[Mo_2O_3\{Rh(aet)_3\}_3]^{4+}$ (**7**)	
Infrared spectra	3428br 3206vs 3116vs 2923w 1582s 1453w 1419m 1302w 1270m 1234w 1133m 1102w 1035w 977m 949s 918w 847w 731w 657w 519w 423w 404w
Raman spectra	1826br 1692w 1598w 1459m 1378w 1307w 1274w 1243w 1163w 1137w 1105w 1046w 978w 956m 943vs 925w 902w 851w 789w 734m 662m 541w 530w 482w 449s 425m 391s 363w 330w 278w 270w 248s 207vs
$[Mo_2O_4\{Co(aet)_3\}_2]^{2+}$ (**8**)	
Infrared spectra	3528w 3452br 3278w 3230s 3119m 2929w 1638w 1594m 1573m 1449w 1385vs 1300w 1265m 1121m 1091m 1034m 973m 930s 915w 839w 720m 668w 527w 454w
Raman spectra	1836br 1656w 1579w 1557w 1456w 1432w 1306w 1271w 1130w 1113w 1054m 978w 934vs 919w 843w 711m 674m 528w 449m 429w 377vs 361s 328s 301m 286vs 249vs 207m 160w 134m

The vibrational spectral data for the present molybdenum-containing complexes are listed in Table 4-14. The infrared spectral pattern of **5** coincides well with that of **6**, reflecting the structural similarity (Table 4-14). On the other hand, the infrared spectrum of **7** exhibits a characteristic strong band at 949 cm^{-1}, which attributes to the symmetric stretching vibration mode of the Mo-O double bonds, and similar band was not observed in those of **5** and **6**. The Raman spectrum of **7** indicates the corresponding band at 943 cm^{-1}. It seems that the band at 734 cm^{-1} is also due to $Mo_2O_3^{4+}$ unit, comparing with those of *fac(S)*-[Rh(aet)$_3$] (Table 3-8). The magnetic moment at room temperature of **5** (2.71 B.M.) is in agreement with that expected from the central Mo^{IV}, which has d^2 electronic structure. However, **6** has lower magnetic moment (2.04 B.M.) than that expected from the central Mo^{III}, which has d^3 electronic structure. It was reported that the molybdenum(III) complexes with some nitrogen donors exhibit magnetic moment of 3.64 - 3.74 B.M..[26] The low magnetic moment of **6** might be considered that three unpaired d electrons are partially delocalized on the three metal ions and interact one another. The pentanuclear complex **7** indicates diamagnetism although it contains Mo^{V}, which have d^1 electronic structure. The molybdenum polynuclear complexes containing $Mo_2O_3^{4+}$ or $Mo_2O_4^{2+}$ unit commonly showed low or non-magnetic moment.[8,27] The long Mo-Mo distance (3.664(1) Å) implies the absence of direct metal-metal interaction, that is, superexchange coupling through the bridging oxo oxygen atom.

The plasma emission spectral analysis for **8** indicated a value of Mo : Co = 1 : 1. The elemental analytical data for nitrate salt of **8** is good agreement with the compositional formula, $\{MoO_2Co(aet)_3(NO_3)\cdot 1.5H_2O\}_n$. In this formula, the complex contains paramagnetic Mo^{V}, which is d^1 type metal ion. However, the magnetic moment at room temperature of **8** indicated its diamagnetism, and the ^{13}C NMR spectrum of **8** gave sharp signals. These suggest that metal-metal interaction or superexchange coupling exists in the complex, and **8** contains more than two molybdenum ion. Moreover, the infrared spectrum of **8** exhibits a characteristic strong band at 930 cm^{-1}, which attributed to the symmetric stretching vibration mode of the Mo-O double bonds (Table 4-14). Similarly, the Raman spectrum of **8** indicates the

corresponding band at 934 cm^{-1}. The strongest infrared band at 1385 cm^{-1} would be due to the nitrate anions. Since $Mo_2O_2(\mu\text{-}O)_2^{2+}$ unit is usually known, the formula of **8** may be $[Mo_2O_4\{Co(aet)_3\}_2](NO_3)_2 \cdot 3H_2O$. The ^{13}C NMR spectrum of **8** is shown in Figure 4-7, and the chemical shifts are listed in Table 4-15, together with the related polynuclear complexes, *meso*- and *rac*-$[Co\{Co(aet)_3\}_2]^{3+}$.[28] As shown in Figure 4-7, **8** exhibits six signals, that is, three signals are in lower field ($\delta > 50$ ppm) and the other three signals are appeared in higher field ($\delta < 40$ ppm). The ^{13}C NMR spectra of *meso*- and *rac*-$[Co\{Co(aet)_3\}_2]^{3+}$ give only two signals due to two kinds of methylene carbon atoms of three aet ligands. Since these are the carbon atom adjacent

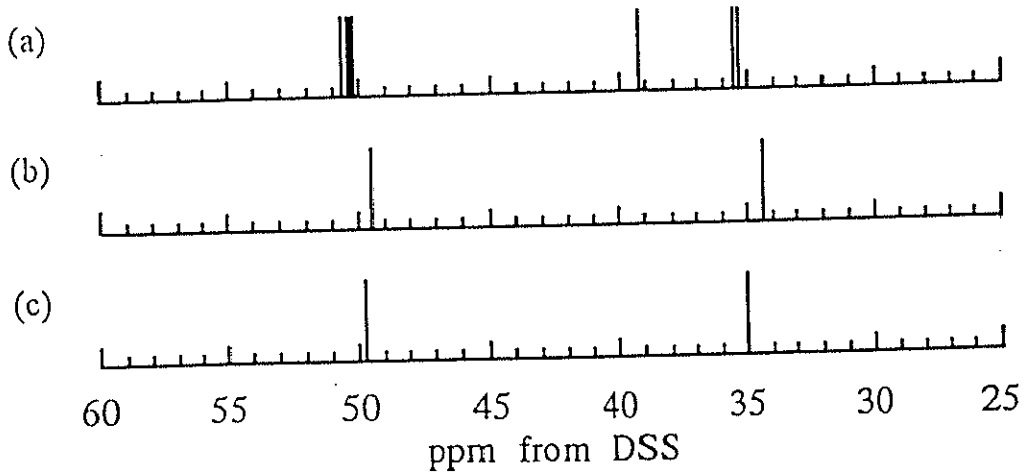

Figure 4-7. ^{13}C NMR spectra of (a) $[Mo_2O_4\{Co(aet)_3\}_2]^{2+}$ (**8**), (b) *meso*-$[Co\{Co(aet)_3\}_2]^{3+}$, and (c) *rac*-$[Co\{Co(aet)_3\}_2]^{3+}$ in D_2O.

Table 4-15. ^{13}C NMR Chemical Shifts[a] of $[Mo_2O_4\{Co(aet)_3\}_2]^{2+}$ (**8**) and $[Co\{Co(aet)_3\}_2]^{3+}$

	NH_2CH_2			SCH_2		
$[Mo_2O_4\{Co(aet)_3\}_2]^{2+}$ (**8**)	50.64	50.39	50.20	39.20	35.57	35.34
meso-$[Co\{Co(aet)_3\}_2]^{3+}$ [b]	49.52			34.40		
rac-$[Co\{Co(aet)_3\}_2]^{3+}$ [b]	49.73			35.05		

a) In ppm from DSS. b) Ref. 28.

to the amino group and the carbon atom adjacent to the bridging sulfur atom, the signals of the former shift to lower field than those of the latter.[28] In the ^{13}C NMR spectrum of **8**, three signals in lower field ($\delta > 50$ ppm) and the other three signals in higher field ($\delta < 40$ ppm) are assigned to the methylene carbon atoms adjacent to the amino group and those adjacent to the sulfur atom of the aet ligands. Consequently, the proposed structure of $[Mo_2O_4\{Co(aet)_3\}_2]^{2+}$ (**8**) is shown in Figure 4-8. Certainly, the molar conductivity of the nitrate salt of **8** in water gave the value of 234 S cm^2 mol^{-1}, and this is close to the value of the known divalent complexes (chapter 3). The complex cation **8** consists of two octahedral *fac(S)*-$[Co(aet)_3]$ units and an oxomolybdenum dinuclear $Mo_2O_2(\mu\text{-}O)_2^{2+}$ moiety, bridged by two oxygen atoms. Each of the two *fac(S)*-$[Co(aet)_3]$ units binds by a triple sulfur-bridge to this $Mo_2O_4^{2+}$ moiety, completing the *S*-bridged boat-type $Co^{III}_2Mo^{V}_2$ tetranuclear structure. The ^{13}C NMR spectra of **8** indicated that the signal at 39.20 ppm shifts ca. 4 ppm from other two signals in higher field. It can be considered that this signal is assigned to the methylene carbon atoms adjacent to the sulfur atoms, which are *trans* to Mo-O double bonds.

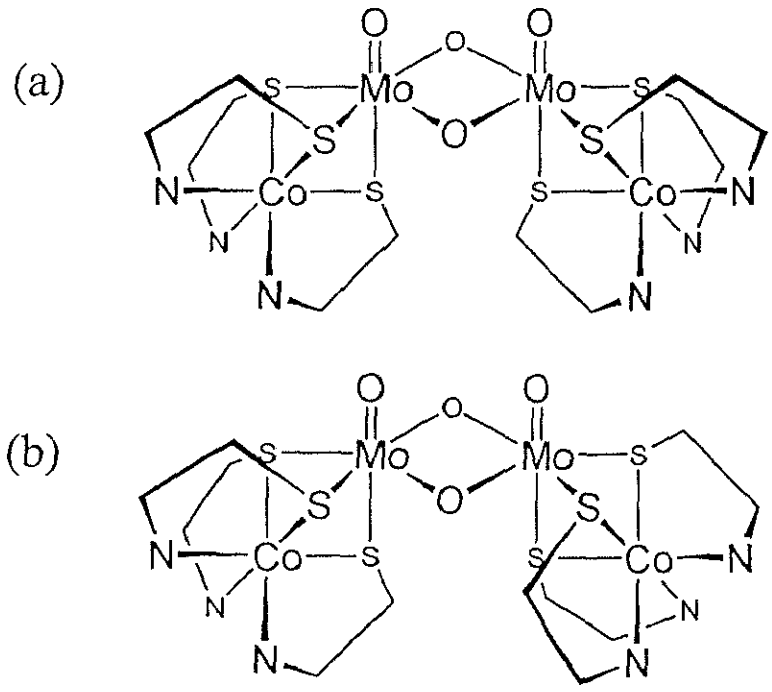

Figure 4-8. Proposed structure of $[Mo_2O_4\{Co(aet)_3\}_2]^{2+}$ (**8**); (a) meso form and (b) racemic form.

In this present tetranuclear complex, two geometrical isomers (meso and racemic forms) are possible (Figure 4-8). The meso isomer has a mirror involving two bridged oxygen atoms and the racemic isomer has a two-fold axis through the center of Mo_2O_2 four-membered ring. Considering the steric hinderance between two methylene carbon atoms adjacent to the sulfur atoms, which are *trans* to Mo-O double bonds of the molecular models, the racemic form is less hindered than that for the meso form. The boat-type tetranuclear complexes, $[\{Co_2(aet)_2\}\{Co(aet)_3\}_2]^{4+}$, in which two *fac(S)*-$[Co(aet)_3]$ units binds to $[Co_2(aet)_2]^{4+}$ moiety, were obtained as two pairs of racemic isomers.[29] Accordingly, $[Mo_2O_4\{Co(aet)_3\}_2]^{2+}$ (**8**) would be the racemic isomer.

The electronic absorption spectra of 7 and 8 are shown in Figure 4-9.

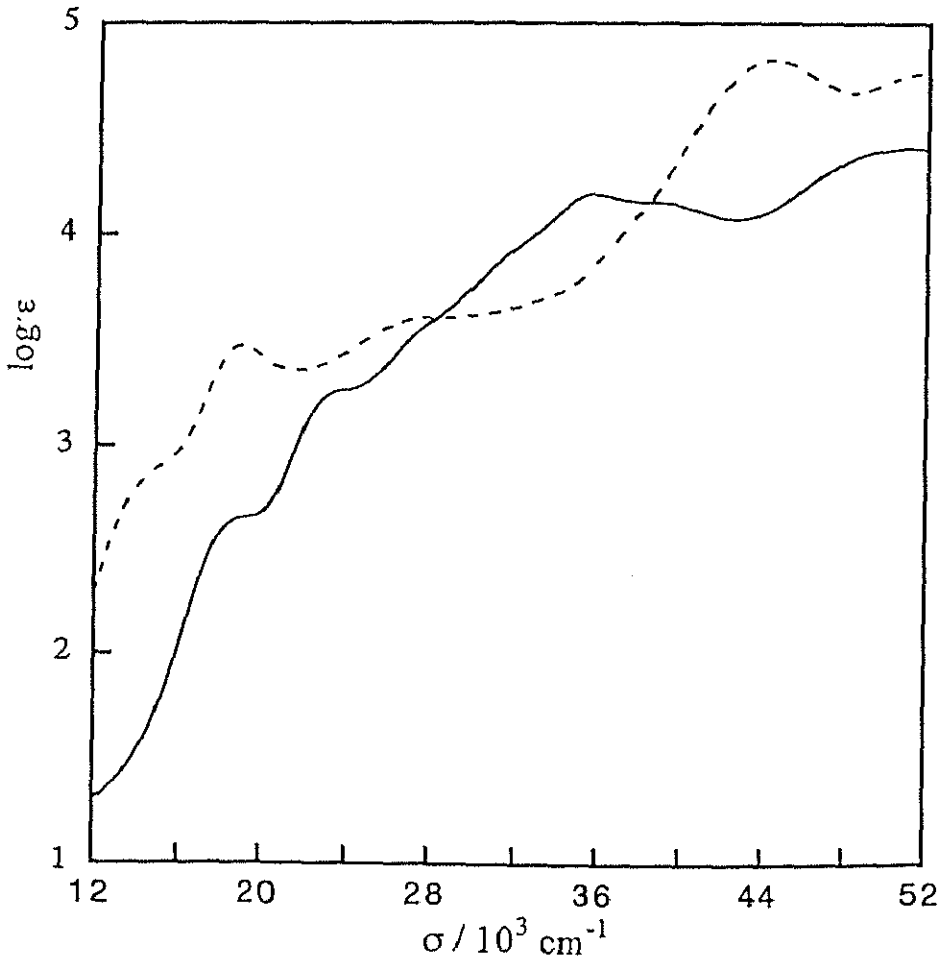

Figure 4-9. Electronic absorption spectra of $[Mo_2O_3\{Rh(aet)_3\}_3]^{4+}$ (7; – – – –) and $[Mo_2O_4\{Co(aet)_3\}_2]^{2+}$ (8; ————).

The ε values of the absorption spectra of the complexes were halved by considering the number of molybdenum in their complexes. The diffuse reflectance as well as absorption spectral data are summarized in Table 4-11. The absorption spectra of 8 exhibits characteristic bands in ca. 20 - 32 x 10^3 cm^{-1} due to the $Mo_2O_4^{2+}$ moiety.[3] However, these bands almost covered with the bands as arising from the terminal *fac(S)*-[$Co(aet)_3$] units.[28] On the other hand, the characteristic bands in lower energy region of 7 (< ca. 25 x 10^3 cm^{-1}) would be due to the molybdenum core, taking account of the absorption spectral behavior of *fac(S)*-[$Rh(aet)_3$].[12] Absorption spectral bands for **8** in water are observed at similar position to the bands of diffuse reflectance spectrum (Table 4-11). This indicates that **8** retains the tetranuclear structure in solution, and it is supported by the results of ^{13}C NMR spectrum and molar conductivity. However, the absorption spectrum for **7** shows shoulder (28.3 x 10^3 cm^{-1}) at different position which is observed in diffuse reflectance spectrum (21.2 x 10^3 cm^{-1}). Moreover, the ^{13}C NMR spectrum of **7** indicates the paramagnetism of this complex in solution, in spite of diamagnetism in solid. These facts suggest that the S-bridged $Rh^{III}_3Mo^{V}_2$ pentanuclear structure of **7** is unstable in solution, converting at least in part to another S-bridged polynuclear structure.

4-3-3. Electrochemical Reactivity

The reaction of *fac(S)*-[$Ir(aet)_3$] with a half equivalent of molybdenum(III) exposed to air in acid at room temperature gave the linear-type S-bridged trinuclear $Ir^{III}Mo^{IV}Ir^{III}$ complex, *meso*-$[Mo^{IV}\{Ir(aet)_3\}_2]^{4+}$ (**5**) (Scheme 4-1). The central molybdenum ion, which does not retain the trivalent of the starting mononuclear complex, is incorporated as tetravalent in the polynuclear structure. Since similar reaction under nitrogen atmosphere also produced complex **5**, the oxidation of molybdenum ion in this reaction would be proceeded by acid as observed in the produce of $[Ir_2(aet)_4(cysta)]^{2+}$ (chapter 3).[30] On the other hand, the reaction of *fac(S)*-[$Rh(aet)_3$] with molybdenum(III) in acid under both nitrogen and air atmosphere at room temperature gave the linear-type S-bridged trinuclear $Rh^{III}Mo^{III}Rh^{III}$ complex,

rac-$[Mo^{III}\{Rh(aet)_3\}_2]^{3+}$ (6) (Scheme 4-1). In this reaction, the central molybdenum ion retains the trivalent of the starting mononuclear complex. Thus, these trinuclear complexes containing one central molybdenum ion, whose valence are different from each other, seem to depend upon terminal building blocks. Attempts to prepare the corresponding polynuclear complexes by the reaction of the molybdenum(III) ion with *fac(S)*-$[Co(aet)_3]$ or *fac(S)*-$[Cr(aet)_3]$ were not successful, as well as the reaction with chromium(III) ion (chapter 2) and oxidizing agents (chapter 3). In the present trinuclear complexes involving the central molybdenum ion, only meso or racemic isomer was obtained. These are in contrast to the fact that both isomers of the corresponding trinuclear $MCr^{III}M$ complexes, *meso*- and *rac*-$[Cr^{III}\{M(aet)_3\}_2]^{3+}$ (M = Ir^{III} and Rh^{III}), were formed by the reaction of *fac(S)*-$[M(aet)_3]$ with chromium(III) (chapter 2).[10] Since the calculated structural energies (MM2 program) for S-bridged trinuclear complexes indicate little difference between isomers (Table 4-16), it may be due to the difference of solubility similar to the case of $[Ni\{Rh(aet)_3\}_2]^{2+}$.[19,31,32]

Table 4-16. Structural Energy Calculations (E / kJ mol^{-1}) of $[Mo\{M(aet)_3\}_2]^{n+}$

	Ir complexes	Rh complexes
$\Delta\Lambda$-isomer	-457.1	-463.8
$\Delta\Delta/\Lambda\Lambda$-isomer	-458.4	-465.0

The trinuclear complexes **5** and **6** were obtained by the reaction under both nitrogen and air atmosphere. However, in the reaction of *fac(S)*-$[Rh(aet)_3]$ with molybdenum(III) in acid under air atmosphere at room temperature, the color of reaction mixture was changed from green-brown to wine-red gradually. From the wine-red suspension, unprecedented S-bridged pentanuclear $Rh^{III}{}_3Mo^{V}{}_2$ complex, $[Mo^{V}{}_2O_3\{Rh(aet)_3\}_3]^{4+}$ (7) was obtained (Scheme 4-1). In the similar reaction under nitrogen atmosphere, the color of reaction mixture retained green-brown at least for 1 d. Namely, the Mo^{III}

Scheme 4-1.

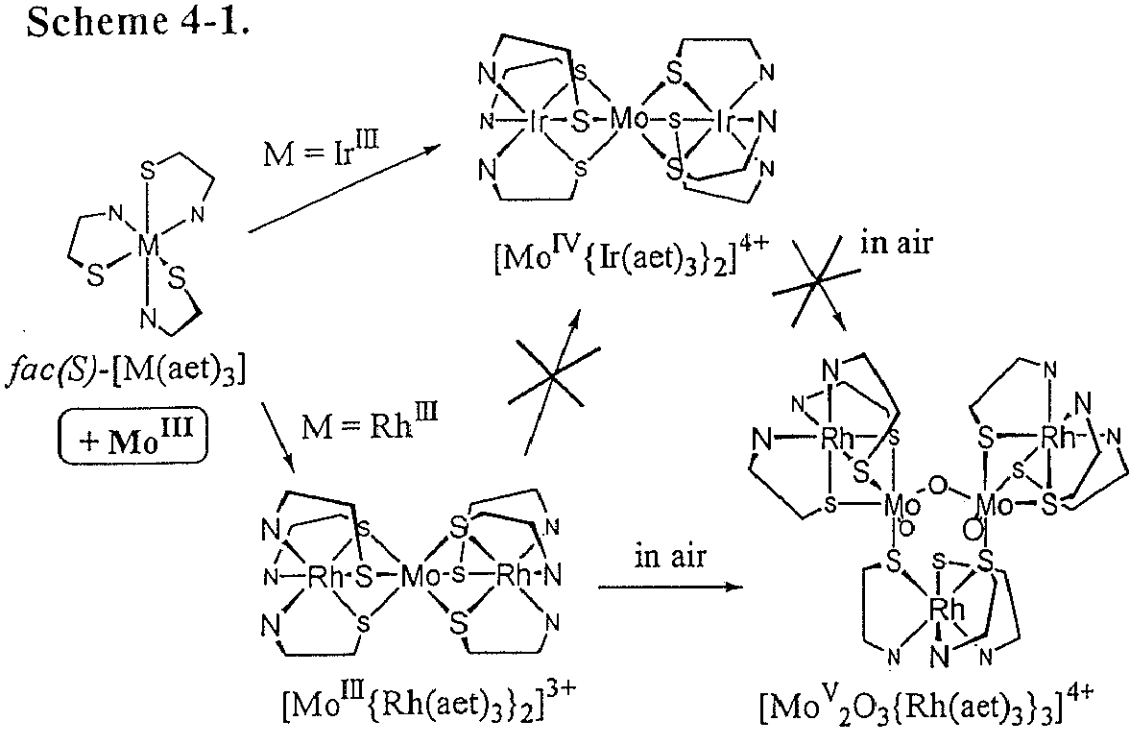

complex **6** is spontaneously oxidized by air and changed to the Mo^{V} complex **7**. It was reported that the $Mo_2O_4^{2+}$ species are preponderant in dilute (ca. 1 mol dm^{-3}) acid condition.[33] For instance, it could be considered tetranuclear structure, $[Mo^{V}_2O_4\{Rh(aet)_3\}_2]^{2+}$. However, **7** has $Mo_2O_3^{4+}$ unit, which predominates in 3 - 5 mol dm^{-3} acid solution, forming more complicated pentanuclear structure, $[Mo^{V}_2O_3\{Rh(aet)_3\}_3]^{4+}$. The present structure would be controlled by *fac(S)*-$[Rh(aet)_3]$ units as building blocks.

Structural conversion from the trinuclear $Rh^{III}Mo^{III}Rh^{III}$ complex **6** to the pentanuclear $Rh^{III}_3Mo^{V}_2$ complex **7** in water was monitored by their absorption spectra. The absorption spectra of **6** and **7** showed the characteristic intense bands at 473 and 529 nm (21.16 x 10^3 and 18.90 x 10^3 cm^{-1}; Table 4-13), respectively. When the aqueous solution containing **6** was stirred at room temperature in air, the color changed from green-brown to wine-red for time. As shown in Figure 4-10, the absorbance at 473 nm for **6** decreased and that at 529 nm for **7** increased. This indicates that the trinuclear $Rh^{III}Mo^{III}Rh^{III}$ complex **6** is converted into the pentanuclear $Rh^{III}_3Mo^{V}_2$ complex **7** by spontaneous oxidation. In this oxidation reaction,

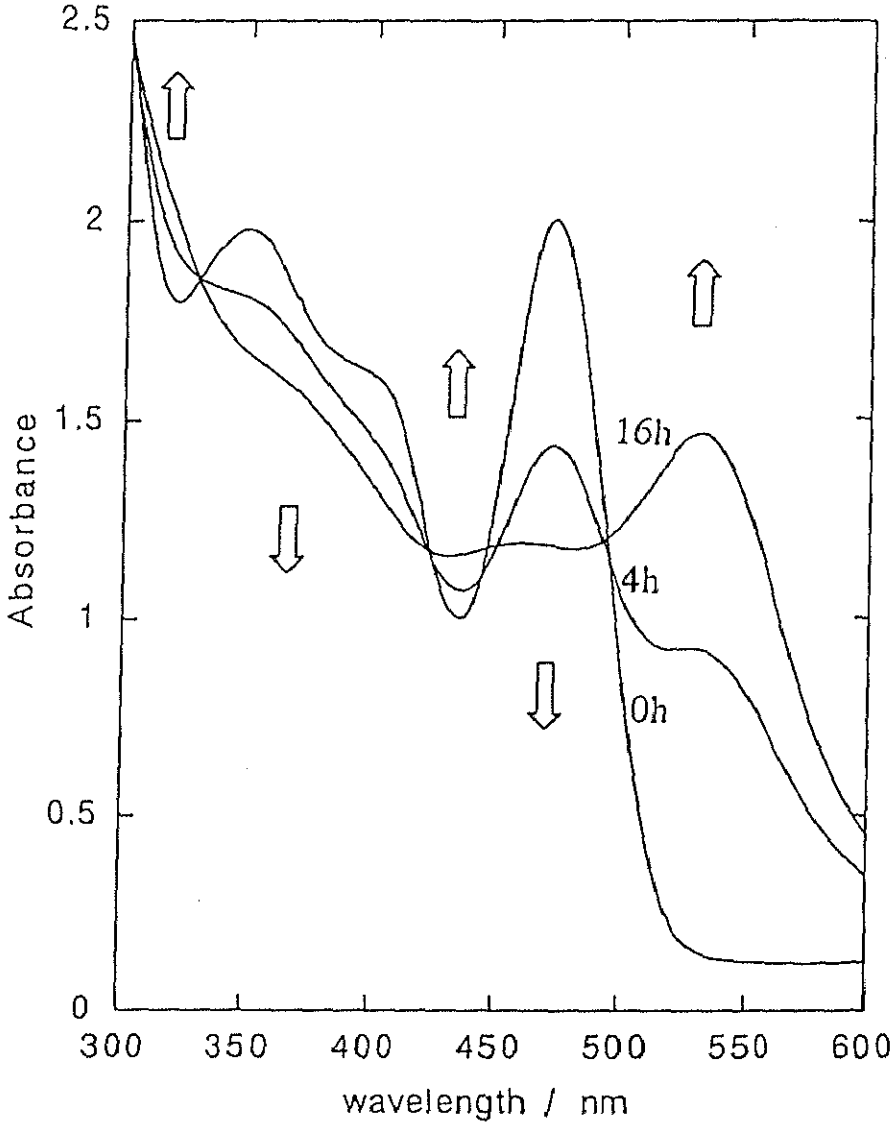

Figure 4-10. Absorption spectral changes with times of $[Mo\{Rh(aet)_3\}_2]^{3+}$ (6).

since the ratio of rhodium and molybdenum in polynuclear structure changes from 2 : 1 to 3 : 2, the resulting excess *fac(S)*-$[Rh(aet)_3]$ was deposited as yellow powder. Although similar experiment for the trinuclear $Ir^{III}Mo^{IV}Ir^{III}$ complex 5 was also attempted, formation of its corresponding pentanuclear complex could not be observed (Scheme 4-1).

Electrochemical studies were performed for $[Mo^{IV}\{Ir(aet)_3\}_2]^{4+}$ (5) and $[Mo^{III}\{Rh(aet)_3\}_2]^{3+}$ (6) in 0.1 mol dm^{-3} Na_2SO_4 aqueous solution. As shown in Figure 4-11, the cyclic voltammogram for $[Mo^{IV}\{Ir(aet)_3\}_2]^{4+}$ (5) displays a quasi-reversible redox process at almost near 0 V, while that for

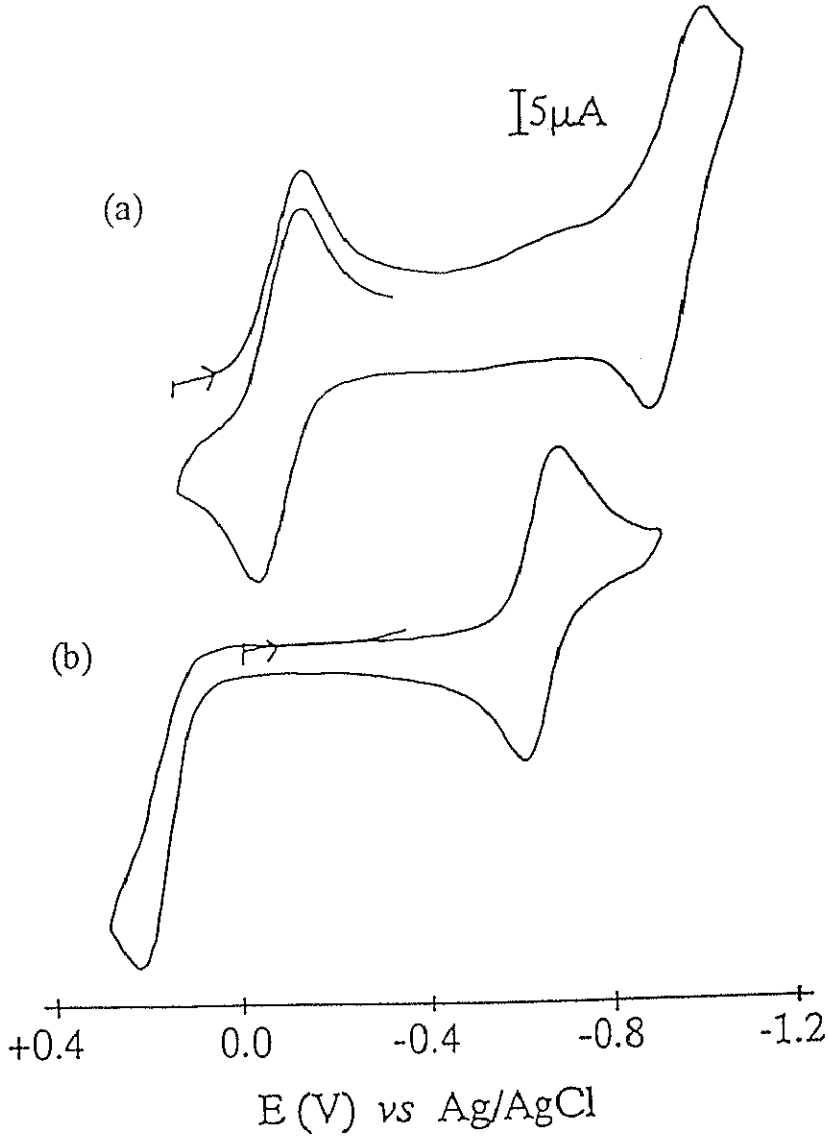

Figure 4-11. Cyclic voltammograms of (a) $[Mo\{Ir(aet)_3\}_2]^{4+}$ (**5**) and (b) $[Mo\{Rh(aet)_3\}_2]^{3+}$ (**6**); scan rate 200 mV s^{-1}; in 0.1 mol dm^{-3} Na_2SO_4 aqueous solution.

$[Mo^{III}\{Rh(aet)_3\}_2]^{3+}$ (**6**) displays an irreversible oxidation wave at more positive potential region. On the other hand, in a negative potential region, a quasi-reversible redox process displayed for both **5** and **6**. Since it has been known that the redox process concerned with the terminal *fac(S)*-$[Ir(aet)_3]$ or *fac(S)*-$[Rh(aet)_3]$ subunits does not occur in the region for their corresponding trinuclear complexes (chapter 2), all displayed waves can be regarded as redox processes of the central molybdenum ion. The quasi-reversible redox processes at a negative potential region ($E^{0'}$ = - 0.96 V, E_{pa} = - 0.88 V, E_{pc} = -

1.00 V for **5** and $E^{0'}$ = - 0.65 V, E_{pa} = - 0.61 V, E_{pc} = - 0.69 V for **6**) probably involve Mo(III)/Mo(II) redox processes. This is in contrast to the fact that Cr(III)/(II) processes of the corresponding $Ir^{III}Cr^{III}Ir^{III}$ and $Rh^{III}Cr^{III}Rh^{III}$ complexes are irreversible (see Figure 2-7). It seems to be indicated that the quasi-reversible redox process ($E^{0'}$ = - 0.08 V; E_{pa} = - 0.03 V; E_{pc} = - 0.13 V) for $Ir^{III}Mo^{IV}Ir^{III}$ complex **5** would involve the central Mo(IV)/Mo(III) redox process. From the potential differences of oxidation waves, it is reasonable to assume that the trivalent molybdenum ion in **6** is relatively stabilized. Moreover, **5** can exist as trinuclear complex involving tetravalent molybdenum ion, while **6** cannot retain the trinuclear structure by oxidation. Namely, **6** is converted into **7** , which has the pentanuclear structure. This fact is in good agreement with the fact that the oxidation wave (E_{pa} = + 0.23 V) is irreversible. Its oxidation potential also indicated that **6** is easily oxidized to **7**. Thus, the cyclic voltammetry experiments obviously showed the electrochemical difference in molybdenum polynuclear complexes depending upon the building blocks.

The reaction of *fac(S)*-$[Co(aet)_3]$ with an equivalent of molybdenum(V) exposed to air in acid at room temperature gave the boat-type S-bridged tetranuclear $Co^{III}{}_2Mo^{V}{}_2$ complex, $[Mo^{V}{}_2O_4\{Co(aet)_3\}_2]^{2+}$ (**8**), which involve a $Mo_2O_2(\mu\text{-}O)_2{}^{2+}$ unit (Scheme 4-2). In this reaction, however, considerable amounts of unidentified materials were accompanied. These insoluble materials may be polymer complexes. The corresponding tetranuclear $Rh^{III}{}_2Mo^{V}{}_2$ or $Ir^{III}{}_2Mo^{V}{}_2$ complexes using *fac(S)*-$[Rh(aet)_3]$ or *fac(S)*-$[Ir(aet)_3]$, respectively, could not isolated at similar condition. Indeed, it seemed that the pentanuclear $Rh^{III}{}_3Mo^{V}{}_2$ or $Ir^{III}{}_3Mo^{V}{}_2$ complexes, which involve a $Mo_2O_2(\mu\text{-}O)^{4+}$ unit, probably formed from their absorption spectral behavior of reaction mixture (Scheme 4-2). Although the pentanuclear $Ir^{III}{}_3Mo^{V}{}_2$ complex has not obtained by the reaction of *fac(S)*-$[Ir(aet)_3]$ with molybdenum(III) ion exposed to air, the direct reaction using molybdenum(V) ion may give the pentanuclear complex. These molybdenum(V) containing polynuclear structures would be controlled by the difference of the building blocks. In addition, these polynuclear complexes may act as catalysts. For example, although $Ir^{III}{}_3Mo^{V}{}_2$ complex has not been isolated, its crude mixture

converted to the dinuclear iridium complex. This complex has two coordinated bridging disulfide bonds, which could not formed by general oxidation reaction. It might be due to the stereochemical interaction, and the investigation[34] is now in progress.

Scheme 4-2.

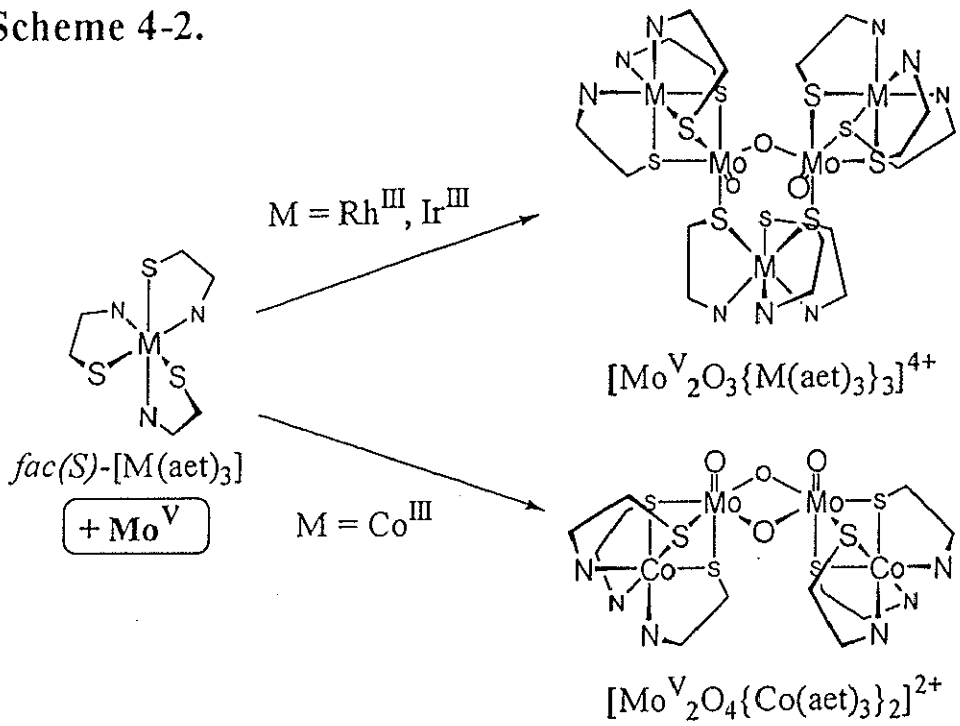

4-3-4. Stereochemistry of Trinuclear Complexes

As shown in Figure 4-6, the present trinuclear complexes, $[M'\{M(aet)_3\}_2]^{n+}$ (M = Ir^{III}, M' = Mo^{IV} (**5**); and M = Rh^{III}, M' = Mo^{III} (**6**)) indicate the characteristic intense bands in the relatively lower energy region ($\sigma <$ ca. 23 x 10^3 cm^{-1}, log $\varepsilon >$ ca. 2.5). Moreover, M'-M distances in the complexes (2.7469(7) Å for **5** and 2.860(3) Å for **6**) are significantly shorter than those in the reported linear-type S-bridged trinuclear structures.[10,19,20] Almost all corresponding complexes, whose crystal structures have been determined so far, have long M'-M distances (> 2.9 Å). In order to elucidate the relationship between metal-metal interaction and absorption bands in the lower energy region, crystal structures of the related complexes were determined. Namely, $[Fe\{Rh(aet)_3\}_2]^{3+}$ indicates the characteristic bands in

the lower energy region,[11] while $[Co\{Rh(aet)_3\}_2]^{3+}$ does not.[12] Selected bond distances and angles for the linear-type S-bridged trinuclear complexes are summarized in Table 4-17. The M'-Rh distance (2.8411(4) Å) of $[Fe\{Rh(aet)_3\}_2]^{3+}$ is shorter than that (2.9098(5) Å) of $[Co\{Rh(aet)_3\}_2]^{3+}$. In the complexes involving the short M'-M distances, obtuse S-M-S angles and

Table 4-17. Selected Bond Distances (Å) and Angles (°) for Linear-Type S-Bridged Trinuclear Complexes, $[M'\{M(aet)_3\}_2]^{n+}$

M'	M	M'-M	M'-S	M-S	M-N	Ref.
Mo^{IV}	Ir^{III}	2.7469(7)	2.458(7)	2.341(7)	2.10(2)	This work
Cr^{III}	Ir^{III}	2.9096(3)	2.421(2)	2.330(2)	2.117(6)	This work
Co^{III}	Ir^{III}	2.906(1)	2.297(2)	2.307(2)	2.120(8)	20
Mo^{III}	Rh^{III}	2.860(3)	2.44(1)	2.33(1)	2.09(4)	This work
V^{III}	Rh^{III}	2.838(1)	2.421(2)	2.321(3)	2.132(8)	35
Cr^{III}	Rh^{III}	2.9328(2)	2.4110(8)	2.3232(8)	2.111(3)	This work
Fe^{III}	Rh^{III}	2.8411(4)	2.306(2)	2.313(2)	2.114(6)	This work
Co^{III}	Rh^{III}	2.9098(5)	2.291(2)	2.307(2)	2.122(7)	This work
Ni^{II}	Rh^{III}	2.9451(5)	2.430(1)	2.323(1)	2.121(4)	19
Co^{III}	Co^{III}	2.857(1)	2.262(11)	2.238(7)	1.996(8)	34
Ni^{II}	Co^{III}	2.930(1)	2.400(1)	2.253(1)	2.005(4)	31
Ni^{II}	Cr^{III}	2.9169(8)	2.425(1)	2.370(2)	2.121(5)	32

M'	M	S-M'-S	S-M-S	N-M-N	M'-S-M	Ref.
Mo^{IV}	Ir^{III}	87.7(2)	93.3(2)	92.1(9)	69.8(2)	This work
Cr^{III}	Ir^{III}	84.36(6)	88.45(6)	95.1(2)	75.51(5)	This work
Co^{III}	Ir^{III}	84.7(1)	84.2(1)	96.3(3)	78.3(1)	20
Mo^{III}	Rh^{III}	85.3(4)	90.3(4)	93(1)	73.6(3)	This work
V^{III}	Rh^{III}	85.54(8)	90.18(9)	95.0(3)	73.49(8)	35
Cr^{III}	Rh^{III}	83.69(3)	87.63(3)	95.5(1)	76.53(2)	This work
Fe^{III}	Rh^{III}	86.30(5)	85.96(6)	95.8(2)	75.91(5)	This work
Co^{III}	Rh^{III}	84.58(7)	83.84(7)	96.8(2)	78.53(6)	This work
Ni^{II}	Rh^{III}	83.26(4)	88.03(4)	95.1(2)	76.55(4)	19
Co^{III}	Co^{III}	83.5(9)	84.5(8)	94.6(6)	78.8(4)	34
Ni^{II}	Co^{III}	81.26(3)	87.88(4)	92.6(1)	77.99(4)	31
Ni^{II}	Cr^{III}	85.60(5)	88.08(5)	94.0(2)	74.93(5)	32

acute M'-S-M angles are observed. It seems that the short Co-Co distance (2.857(1) Å) of $[Co\{Co(aet)_3\}_2]^{3+}$ [35] is due to both central and terminal Co-S bonds are the shortest in the listed trinuclear complexes (Table 4-17). Additionally, $[V\{Rh(aet)_3\}_2]^{3+}$, which indicates the characteristic intense bands, has also similar V-Rh distance (2.838(1) Å) to the Fe-Rh one.[36] In the trinuclear complexes consist of terminal rhodium units and central trivalent metal ion, which is the first row transition series, the M'-S distances increase in the order of Co^{III}, Fe^{III}, Cr^{III}, and V^{III}. This order is in agreement with that of the ionic radii. However, the M'-M distances in these complexes increase in the order of V^{III}, Fe^{III}, Co^{III}, and Cr^{III}. This inconsistency emphasizes that the central vanadium(III) and iron(III) ions approach the terminal rhodium(III) ions. Moreover, the absorption spectral pattern in lower energy region of $Rh^{III}Mo^{III}Rh^{III}$ complex is not similar to that of corresponding $Rh^{III}Cr^{III}Rh^{III}$ complex (vide supra). It is suggested that the substantial metal-metal interaction via direct metal orbital - metal orbital overlap occurs in $[M'\{Co(aet)_3\}_2]^{3+}$ (M' = Fe^{III} and Ru^{III}) from electron spin resonance study.[37] Accordingly, the characteristic absorption intense bands in the lower energy region of the linear-type S-bridged trinuclear complexes might be due to the central metal - terminal metal interaction.

References and Notes

1) T. Shibahara, *Coord. Chem. Rev.*, **123**, 73 (1993).

2 a) H. Akashi, T, Shibahara, and H. Kuroya, *Polyhedron*, **9**, 1671 (1990); b) G. Sakane, K. Hashimoto, M. Takahashi, M. Takeda, and T. Shibahara, *Inorg. Chem.*, **37**, 4231 (1998); c) C. A. Routledge, M. Humanes, Y. Li, and A. G. Sykes, *J. Chem. Soc., Dalton Trans.*, **1994**, 1275.

3) V. R. Ott, D. S. Swieter, and F. A. Schultz, *Inorg. Chem.*, **16**, 2538 (1977).

4 a) D. Coucouvanis, *Acc. Chem. Res.*, **24**, 1 (1991); b) R. L. Richards, *Coord. Chem. Rev.*, **154**, 83 (1996); c) J. Kim and D. C. Rees, *Science*, **257**, 1677 (1992); d) D. Sellmann, *Angew. Chem. Int. Ed. Engl.*, **32**, 64 (1993).

5 a) M. J. Morris, *Coord. Chem. Rev.*, **152**, 309 (1996); b) M. J. Morris, *Coord.*

Chem. Rev., **164**, 289 (1997).

6 a) J. R. Knox and C. K. Prout, *Acta Crystallogr.*, **B25**, 2281 (1969); b) J. A. Zubieta and G. B. Maniloff, *Inorg. Nucl. Chem. Lett.*, **12**, 121 (1976).

7) P. M. Boorman, H.-B. Kraatz, M. Parvez, and T. Ziegler, *J. Chem. Soc., Dalton Trans.*, **1993**, 433.

8) R. Lozano, J. Román, F. de Jesús, and E. Alarcón, *Trans. Met. Chem.*, **15**, 141 (1990).

9) H. K. Chae, W. G. Klempeter, and T. A. Marquart, *Coord. Chem. Rev.*, **128**, 209 (1993).

10) Y. Miyashita, N. Sakagami, Y. Yamada, T. Konno, J. Hidaka, and K. Okamoto, *Bull. Chem. Soc. Jpn.*, **71**, 661 (1998).

11) S. Aizawa, *Ph. D. Thesis, University of Tsukuba*, **1989**.

12) T. Konno, S. Aizawa, K. Okamoto, and J. Hidaka, *Bull. Chem. Soc. Jpn.*, **63**, 792 (1990).

13) T. Shibahara and M. Yamazaki, *Bull. Chem. Soc. Jpn.*, **63**, 3022 (1990).

14) "Landolt-Börnstein Tabellen", Neue Serie, II Band, 2 Teil, Springer-Verlag (1966).

15) Molecular Mechanics. Version 3.7. CAChe Scientific, Inc, 1994.

16) SAPI91. Fan Hai-Fu (1991). Structure Analysis Programs with Intelligent Control, Rigaku Corporation, Tokyo, Japan.

17) SIR92. A. Altomare, M. C. Burla, M. Camalli, M. Cascarano, C. Giacovazzo, A. Guagliardi, and G. Polidori, *J. Appl. Cryst.*, **27**, 435 (1994).

18) teXsan. Molecular Structure Corporation. Single Crystal Structure Analysis Software. Version 1.8, MSC, 3200 Research Forest Drive, The Woodlands, TX 77381, USA (1997).

19) T. Konno and K. Okamoto, *Bull. Chem. Soc. Jpn.*, **68**, 610 (1995).

20) T. Konno, K. Nakamura, K. Okamoto, and J. Hidaka, *Bull. Chem. Soc. Jpn.*, **66**, 2582 (1993).

21) T. Konno and K. Okamoto, *Inorg. Chem.*, **36**, 1403 (1997).

22) T. Konno, C. Sasaki, and K. Okamoto, *Chem. Lett.*, **1996**, 977.

23 a) T. Konno, K. Okamoto, and J. Hidaka, *Inorg. Chem.*, **30**, 2253 (1991); b) T. Konno, K. Okamoto, and J. Hidaka, *Inorg. Chem.*, **33**, 538 (1994); c) T. Konno, Y. Kageyama, and K. Okamoto, *Bull. Chem. Soc. Jpn.*, **67**, 1957

(1994); d) K. Okamoto, T. Konno, Y. Kageyama, and J. Hidaka, *Chem. Lett.*, **1992**, 1105; e) K. Okamoto, Y. Kageyama, and T. Konno, *Bull. Chem. Soc. Jpn.*, **68**, 2573 (1995); f) K. Okamoto, T. Konno, and J. Hidaka, *J. Chem. Soc., Dalton Trans.*, **1994**, 533.

24) R. H. Holm, *Chem. Rev.*, **87**, 1401 (1987).

25) S. N. Shaikh and J. Zubieta, *Inorg. Chem.*, **27**, 1896 (1988).

26) S. P. Ghosh and K. M. Prasad, *J. Less-Common Metals*, **36**, 223 (1974).

27) J. F. Johnson and W. R. Scheidt, *Inorg. Chem.*, **17**, 1280 (1978).

28) S. Miyanowaki, *Master Thesis, University of Tsukuba*, **1989**.

29 a) T. Konno and K. Okamoto, *Chem. Lett.*, **1995**, 675; b) T. Konno, Y. Gotoh, and K. Okamoto, *Inorg. Chem.*, **36**, 4992 (1997).

30 a) T. Konno, Y. Miyashita, and K. Okamoto, *Chem. Lett.*, **1997**, 85; b) Y. Miyashita, N. Sakagami, Y. Yamada, T. Konno, and K. Okamoto, *Bull. Chem. Soc. Jpn.*, **71**, 2153 (1998).

31) T. Konno, K. Okamoto, and J. Hidaka, *Acta Crystallogr.*, **C49**, 222 (1993).

32) K. Okamoto, M. Matsumoto, Y. Miyashita, N. Sakagami, J. Hidaka, and T. Konno, *Inorg. Chim. Acta*, **260**, 17 (1997).

33) S. Himeno and M. Hasegawa, *Inorg. Chim. Acta*, **83**, L17 (1984).

34) Y. Miyashita, Y. Yamada, K. Kanamori, and K. Okamoto, *Manuscript in preparation.*

35) M. J. Heeg, E. L. Blinn, and E. Deutch, *Inorg. Chem.*, **24**, 1118 (1985).

36) M. Hamajima, *Bachelor Thesis, University of Tsukuba*, **1997**.

37) R. E. DeSimome, T. Ontko, L. Wardman, and E. L. Blinn, *Inorg. Chem.*, 14, 1313 (1975).